Available online at www.sciencedirect.com
SCIENCE DIRECT®
International Journal of Multiphase Flow 30 (2004) 1337–1367
International Journal of Multiphase Flow
www.elsevier.com/locate/ijmulflow

On the locomotion of a drop, induced by the internal secretion of surfactant

Dina Tsemakh, Olga M. Lavrenteva, Avinoam Nir *

Department of Chemical Engineering, Technion-I.I.T., Haifa 32000, Israel

Received 19 October 2003; received in revised form 24 June 2004

Abstract

The locomotion of a viscous drop induced by an internal secretion of a weak surface-active substance is considered. The system consists of a viscous drop that contains another smaller droplet at an off-center location and is embedded in an unbounded viscous fluid that is free of the surfactant far from the drop. The inner droplet has a uniform concentration of the secreted material, while a non-adsorbing kinetics is used for the mass flux across the surface of the larger drop. The mass transfer results in a non-uniform distribution of interfacial tension at the outer surface and induces a Marangoni flow there and a migration of the fluid particles. The dependence of the velocities of the drops migration on the distance between the centers and on governing parameters such as the ratios of the viscosity and diffusivity of the phases is studied for the cases when the motion is induced solely by the Marangoni effect and under the combined action of gravity and thermocapillarity. Non-linear effects of convective transport at low and high Peclet numbers and of surface deformations are presented.

Keywords: Compound drop; Locomotion; Marangoni flow

* Corresponding author. Tel.: +972 4829 2119; fax: +972 839 5672.
E-mail address: avinir@tx.technion.ac.il (A. Nir).

0301-9322/$ - see front matter
doi:10.1016/j.ijmultiphaseflow.2004.06.005

1. Introduction

Drops containing smaller droplets or bubbles (compound drops) are encountered in many modern applications, such as direct-contact heat exchange (Sideman and Moalem-Maron, 1982), membrane separation technology (Landman, 1983), liquid–liquid extraction and so on. Compound drops can also model complex systems such as eukaryotic biological cells (Kan et al., 1998, 1999). Numerous studies of the hydrodynamics of multiphase drops have been stimulated by its extreme technological importance. Sadhal and Oguz (1985) examined the buoyancy driven motion of a non-deformable compound drop and found a rich variety of flow patterns. The effect of small deformations was studied by Landman (1985), Chervenivanova and Zapryanov (1989) and by Stone and Leal (1990) making use of perturbation techniques. Larger deformations in simple shear and extensional flows were studied numerically by Stone and Leal (1990) and by Kan et al. (1998, 1999).

During the processes mentioned above, the motion of the compound drops is typically accompanied by heat or mass transfer and one may expect a significant influence of the Marangoni effect on the dynamics. Thus, the motion of spherical compound drops under externally imposed temperature or surfactant concentration gradient was investigated by Morton et al. (1990). The motion that results from both a temperature field and residual contaminations applied at the surface of a liquid system was analyzed by Lyell and Carpenter (1993).

In some cases the surface of the encapsulated drop may be active, e.g. a surface-active substance may be secreted from it. For an off-center location of the inner drop, the diffusive mass transfer results in a non-uniform distribution of surfactant along the outer surface that, in turn, results in interfacial stress variation that ultimately induce a surface motion and locomotion of the drop. An internal secretion of active substance is typical especially for small biological bodies. The described system may thus serve as a simplified model for chemotaxis of biological particles due to the activity of internal organelles such as mitochondria, lysosomes, and Golgi apparata. On the other hand, the Marangoni convection induced inside the drop results in the migration of the inner droplet in the direction of the surface or the center of the large drop. This effect may stabilize or destabilize a concentric position of the inclusion and thus to be of importance in the processes of encapsulation, etc.

In this paper we present a theoretical study of the motion of the compound drop due to the internal secretion of a surface-active substance. In our model we consider a viscous drop that contains another smaller droplet at an off-center location. The system is embedded in an unbounded viscous fluid that is free of the surfactant far from the drop. The inner droplet has a uniform concentration of the secreted material, while a non-adsorbing kinetics is used for the mass flux across the surface of the larger drop. The focus of the study is on the case of a locomotion induced solely by the Marangoni effect. For completeness, the combined action of buoyancy and Marangoni effect is also considered. Our primary interest is on the motion of small bodies when the surface forces are comparable with mass forces or dominate over them in a quiescent fluid.

In Section 2 a mathematical model of the process is formulated, and the relative influence of inertia, convective mass-transfer and the deformability of the interfaces are discussed. In Section 3 a simplified quasi-stationary model (briefly described in Nir and Lavrenteva, 2003) is presented and the method of solution that used some earlier results of the motion of compound drops (Sadhal and Oguz, 1985; Morton et al., 1990; Loewenberg and Davis, 1993) is described.

The results of calculations for the motion in the absence of external forcing are given in Section 4. It was found that, although the surface of the inner droplet has a uniform concentration, the droplet migrates within the outer body due to the internally induced circulation. In the case, when interfacial tension grows with the concentration of the secreted surfactant, the inner drop migrates to the center of the outer one and, with time, a stable concentric configuration is established. However, if the secreted surfactant reduces the interfacial tension as it happens in most cases, the velocity of the inner droplet exceeds that of the large drop. With the passage of time, the droplet approaches the interface of the drop and the eccentricity of the system is increased. When the distance between the centers increases the relative velocity first grows, but when the droplet approaches the interface its motion is retarded by the strong viscous resistance. At the limiting configuration of touching surfaces the aggregate moves with a constant non-zero velocity. To study the motion of the inner droplet near the interface of the outer one, a use was made of a modification of an approach developed earlier for two separate drops at close proximity (Loewenberg and Davis, 1993). The details of the methods used and the results of the calculations for the spontaneous motion are given in Sections 3.2 and 4, respectively.

In the case of a simultaneous action of buoyancy and a spontaneous Marangoni effect, the inner particle does not necessarily migrate to the surface or center of the outer drop but it may reach a stable eccentric configuration. Possible regimes of interaction and corresponding flow patterns are described in Section 4.2. Our basic results were calculated for the case of non-deforming surfaces where inertia is neglected and when diffusion dominates the mass transfer mechanisms in the bulks. In Section 5 we study the possible effect of unsteady and non-linear convective mass transfer at low and high Peclet numbers, while in Section 6 the effect of slight deformability of the interfaces at various regimes and various stages of the process is analyzed. The conclusions are given in Section 7.

2. Problem formulation

Consider a drop of radius a submerged into an unbounded viscous fluid and containing another smaller droplet of radius b that serves as a source of a soluble weak surfactant. The three different immiscible phases are denoted by the indices 0, 1 and 2 as shown in Fig. 1. Assume further that the ambient fluid far from the drop is quiescent and free of surfactants, and that the concentration of the surfactant on the inner interface, C_2, is uniform. All physical properties of the fluids are assumed to be constant, except for the interfacial tension on the outer interface, which is considered to depend solely on the concentration, $\sigma = \sigma(C)$. This dependence can be established experimentally or deduced theoretically from thermodynamic considerations (see e.g. Edwards et al., 1991 and Chen and Stebe, 1997). In practice, it is often linearized to yield $\sigma = \sigma_0 + \sigma_c C$, with σ_c being a negative constant. Since the concentration in our system varies from zero to C_2, a requirement $|\sigma_c| C_2/\sigma_0 < 1$ is sufficient to ensure positiveness of the surface tension.

At the outset, we introduce dimensionless variables based on the size of the larger drop and on the physical properties of the ambient fluid. The velocity is scaled by $V^* = |\sigma_c| C_2/\eta_0$, where η_0 denotes the ambient fluid viscosity, and the concentration is scaled by C_2. The system is governed by the following set of dimensionless parameters: Reynolds number, $Re = \rho_0 a V^*/\eta_0$, where ρ_0 is the density of the ambient phase; Peclet numbers, $Pe_i = a V^*/D_i$, with D_i being the diffusivity of the

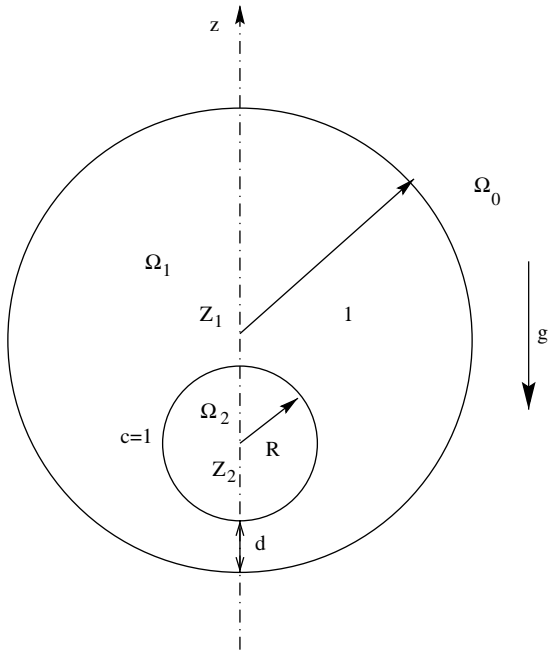

Fig. 1. Schematic illustration of a drop with an eccentrically located inclusion.

surfactant in the liquid i; capillary numbers, $Ca_1 = \eta_1 V^*/\sigma_0$ and $Ca_2 = \eta_2 V^*/\sigma_2$, where η_i is the viscosity of the corresponding phase and σ_2 is the interfacial tension at the inner droplet surface. Denoted are the ratios of physical characteristics of the phases and the ratio of drops' radii by $\mu_i = \eta_i/\eta_0$ ($i = 1,2$), $\kappa = D_1/D_0$ and $R = b/a$, respectively. When the compound drop moves under the action of gravity force, the numbers

$$Ar_1 = \frac{4\pi}{3} g \frac{(\rho_0 - \rho_1)a^3 - (\rho_1 - \rho_2)b^3}{V^* \eta_0 a} \quad \text{and} \quad Ar_2 = \frac{4\pi}{3} g b^3 \frac{\rho_1 - \rho_2}{V^* \eta_0 a},$$

with ρ_i being the density of liquid i and g being the magnitude of gravitational acceleration, characterize the relative influence of gravity and Marangoni effect for each of the drops. Note that these parameters may be negative as well as positive. If the averaged density of the aggregate exceeds that of the ambient liquid, Ar_1 is negative while in the opposite case it is positive.

Our primary interest is in the motion of small bodies ($a \sim 10^{-3}$–10^{-8} m) in an otherwise quiescent fluid when the surface forces are comparable with gravity forces or dominate over them. The characteristic velocity of such a flow is proportional to the drops dimension a and the Reynolds number, being thus proportional to a^2, remains small. The inertia-induced correction to steady and quasi-steady migration velocities of particles in viscous fluid at low Reynolds number is a well-studied subject. Beginning with the classical works by Oseen (1927) and Basset (1888), who considered the motion of a single solid particle in a quiescent fluid, it is believed that the leading effect of inertia scales as Re and $Re^{1/2}$ for the stationary and non-stationary problems, respectively. Recently it was realized (see Leshansky et al., 2003, 2004) that an Oseen-type $O(Re)$ correction is related to an $O(1/|x|)$ term in the far field velocity expansion, Stokeslet, while a Bas-

set-type O ($Re^{1/2}$) correction is related to the time derivative of the Stokeslet. (Though only solid particles were considered, the results are equally applicable to the cases of drops and bubbles.) In the absence of a Stokeslet for surface-induced motion (e.g. Subramanian and Balasubramaniam, 2001), and for a time independent Stokeslet associated with the motion of a collection of particles in gravity field, the expected effect of inertia is even weaker, being of O (Re) for the transient unsteady period and of O (Re^2) for steady configurations. These values are small and, thus, it is anticipated that the solution with $Re = 0$ will be an appropriate approximation.

Under the quasi-steady approximation for the hydrodynamic part of the problem the pressure and velocity fields can be found from stationary Stokes equations for any given configuration of the interfaces and distribution of concentration over the interfaces. The velocity, $\mathbf{u}$, and pressure (modified by adding the gravity force potential), p, fields in each phase satisfy the quasi-stationary Stokes equations

$$\mu_i \nabla^2 \mathbf{u}_i = \nabla p_i, \quad \nabla \cdot \mathbf{u}_i = 0, \quad \mathbf{x} \in \Omega_i, \quad i = 0, 1, 2, \tag{1}$$

and the following boundary conditions are applied: the fluid is at rest at infinity

$$\mathbf{u}_0 \to 0, \quad |\,\mathbf{x}\,| \to \infty, \tag{2}$$

while the velocity field is continuous across the drops' interfaces

$$\mathbf{u}_{0,2} = \mathbf{u}_1, \quad \mathbf{x} \in \partial\Omega_{1,2}. \tag{3}$$

The balance of stresses at the interfaces read

$$(\mathbf{\Pi}^1 - \mathbf{\Pi}^0) \cdot \mathbf{n} = 2(Ca_1^{-1} - c)H\mathbf{n} + \nabla_\tau c, \quad \mathbf{x} \in \partial\Omega_1, \tag{4}$$

$$(\mathbf{\Pi}^2 - \mathbf{\Pi}^1) \cdot \mathbf{n} = 2Ca_2^{-1} H\mathbf{n}, \quad \mathbf{x} \in \partial\Omega_2, \tag{5}$$

Here $\nabla_\tau = \nabla - \mathbf{n}(\mathbf{n} \cdot \nabla)$ denotes a so-called surface gradient, $\mathbf{\Pi}^i = -p_i\mathbf{I} + \mu_i[\nabla\mathbf{u}_i + (\nabla\mathbf{u}_i)^{\mathrm{T}}]$ is the stress tensor, while $\mathbf{n}$ and H are the unit normal vector and mean curvature of the surface, respectively. Note that Ca_1 should not exceed unity to avoid negative surface tension and, thus, it can be considered as a small parameter. Ca_2 is normally of the same order of magnitude as Ca_1.

Since the liquids are immiscible, the normal components of the velocity of each fluid at the surface of a drop and the normal velocity of the interface, U_i, are equal

$$\mathbf{u}_i \cdot \mathbf{n}_i = U_i, \quad \mathrm{x} \in \partial\Omega_i, \quad i = 1, 2. \tag{6}$$

The dimensionless concentration fields c_i satisfy diffusion equation

$$Pe_i(\partial c_i/\partial t + \mathbf{u} \cdot \nabla c_i) = \Delta c_i, \quad \mathbf{x} \in \Omega_i, \quad i = 0, 1. \tag{7}$$

The concentration is constant at the surface of the small drop

$$c_1 = 1, \quad \mathbf{x} \in \partial\Omega_2.$$

The concentration and the mass flux are continuous through the surface of the large drop, i.e.

$$c_1 = c_0, \quad \frac{\partial c_0}{\partial n} = \kappa \frac{\partial c_1}{\partial n}, \quad \mathbf{x} \in \partial\Omega_1.$$

The problem formulation is completed by the initial conditions for the concentration and the geometry of the surfaces of the drops.

In contrast to the Reynolds number that, for the cases under consideration, is always very small and the Capillary number that is smaller than one, the Peclet number may vary from very small up to very large values. In this paper our primary interest is on the case of negligibly small Pe that is considered in Sections 3 and 4. For completeness we consider also the leading order corrections to this solutions in Pe and the case of small Pe inside the drop and large outside, see Section 5.

3. Quasi-stationary motion of spherical drops: method of solution

For negligibly small Peclet number of the both phases, the leading order approximation of the dimensionless concentration fields c_i satisfy Laplace equation

$$\Delta c_i = 0, \quad \mathbf{x} \in \Omega_i, \quad i = 0, 1. \tag{8}$$

The concentration vanishes in the ambient fluid far from the drops

$$c_0 \to 0 \quad |\,\mathbf{x}\,| \to \infty, \tag{9}$$

being constant at the surface of the small drop,

$$c_1 = 1, \quad \mathbf{x} \in \partial\Omega_2. \tag{10}$$

The concentration and the mass flux are continuous through the surface of the large drop, i.e.,

$$c_1 = c_0, \quad \frac{\partial c_0}{\partial n} = \kappa \frac{\partial c_1}{\partial n}, \quad \mathbf{x} \in \partial\Omega_1. \tag{11}$$

The concentration field resulting from problem (8)–(11) may be solved for any given configuration of the system independent of the hydrodynamic part and provide the distribution of concentration on the interface $\partial\Omega_1$.

As soon as the latter is known, the velocity field can be obtained by solving (1)–(5) for a given configuration of the interfaces. The latter then are advances with the normal velocities given by (6). The zero Reynolds and Peclet numbers formulation is addressed as a quasi-stationary approximation since both concentration and velocity field are found from the stationary equations depending on time parametrically via evolving geometry of the interfaces.

If capillary numbers associated with both interfaces are small then, at the leading order, the drops maintain their spherical shape and, hence, the normal components of the velocity of the fluid at the surface of a drop and of the velocity of the drop, $\mathbf{V}_i$, are equal, i.e.

$$U_i = \mathbf{V}_i \cdot \mathbf{n}, \quad \mathbf{x} \in \partial\Omega_i, \quad i = 1, 2. \tag{12}$$

The normal stress balance results in the balance of the forces acting on each of the drops

$$\mathbf{F}_i = \oint_{\partial\Omega_i} \mathbf{\Pi}^i \cdot \mathbf{n} \mathrm{d}s + m_i \mathbf{g} = \mathbf{0}. \tag{13}$$

A correction to the solution of the spherical drops can be constructed using the methods of regular perturbation expansions in capillary numbers. The details are given in Section 6.

If the motion of the droplets is axi-symmetric, as it is in the case of the motion driven solely by the Marangoni effect, it is convenient to apply orthogonal coordinates, (ξ, η, ϕ), conjugate to the cylindrical system (z, r, ϕ), having the interfaces of the drops as coordinate surfaces and to introduce an axi-symmetric Stokes stream function Ψ such that the velocity components are

$$u_\xi = \frac{h}{r}\frac{\partial \Psi}{\partial \zeta}, \quad u_\zeta = -\frac{h}{r}\frac{\partial \Psi}{\partial \xi},$$

where h is a metric coefficient.

The stream function satisfies the following equation (Happel and Brenner, 1965):

$$E^2(E^2\Psi_i) = 0, \quad \mathbf{x} \in \Omega_i, \quad i = 0, 1, 2 \tag{14}$$

with

$$E^2 = rh^2\left[\frac{\partial}{\partial \xi}\left(\frac{1}{r}\frac{\partial}{\partial \xi}\right) + \frac{\partial}{\partial \zeta}\left(\frac{1}{r}\frac{\partial}{\partial \zeta}\right)\right]$$

In this representation the subscripts 0, 1 and 2 correspond to domains of the continuous outer phase with $\xi < \alpha$, the larger drop, $\alpha < \xi < \beta$, and the droplet, $\xi > \beta$, respectively.

The boundary conditions (3), (6) can be rewritten in terms of the stream function as

$$\Psi_{0,2} = \Psi_1 = -r^2 V_{1,2} \quad \text{and} \quad \frac{\partial \Psi_{0,2}}{\partial \xi} = \frac{\partial \Psi_1}{\partial \xi}, \quad \xi = \alpha, \beta. \tag{15}$$

The tangential stresses balances at the interface of the drops, which link the concentration and the velocity fields, are of the form

$$\mathbf{\Pi}^0_{\xi\zeta} - \mathbf{\Pi}^1_{\xi\zeta} = h\frac{\partial c}{\partial \zeta}, \quad \xi = \alpha, \tag{16}$$

$$\mathbf{\Pi}^1_{\xi\zeta} - \mathbf{\Pi}^2_{\xi\zeta} = 0, \quad \xi = \beta. \tag{17}$$

As soon as the stream function is known, the force exerted on a body by the fluid in the positive z-direction can be calculated as (Happel and Brenner, 1965)

$$F_z = \mu\pi \int r^3 \frac{\partial \Psi}{\partial \xi}\left(\frac{E^2\Psi}{r^2}\right)\mathrm{d}\zeta. \tag{18}$$

Due to the linearity of the problem, the flow field may be constructed as a superposition of a Marangoni flow generated around the interfaces of the drops at rest by a given distribution of surfactants and a flow that would be generated by the motion of the drops in the absence of the Marangoni effect. Similarly, the force acting on each drop can be represented as a sum of the following forces:

1. Marangoni force F_i^{m} that is exerted on the drop i at rest by a flow generated by a non-uniform distribution of concentration. Supposing $V_1 = V_2 = 0$ in boundary condition (15) we solve the system of Eqs. (15)–(17) and then find the force F_i^{m} according to formula (18).

2. Hydrodynamic drag force, $V_1 F_i$, that acts on a moving drop in the presence of another drop moving with the same velocity V_1 and in the absence of the Marangoni effect. F_i can be found by applying (18) to the solution of (15)–(17), with $V_1 = V_2 = 1$ and with $\partial c/\partial\zeta = 0$ in boundary condition (16).
3. Hydrodynamic force, $V_r F_r$, that acts on a droplet moving with the velocity V_r within the quiescent outer drop in the absence of the Marangoni effect. F_r can be found by applying (18) to the solution of (15)–(17), with $V_1 = 0$, $V_2 = 1$, and with $\partial c/\partial\zeta = 0$ in boundary condition (16).
4. Gravity and buoyancy forces exerted on the particles, $F_i^{\mathrm{g}} = Ar_i$, $i = 1,2$.

If the drops do not touch, the balances of the forces acting on the drops are

$$V_1 F_1 + F_1^{\mathrm{g}} + F_1^{\mathrm{m}} = 0, \tag{19}$$

$$V_1 F_2 + V_r F_r + F_2^{\mathrm{g}} + F_2^{\mathrm{m}} = 0 \tag{20}$$

and they provide a system of linear algebraic equations for the velocities of the particles. A modification of these force balances in the case of drops in contact is discussed below in Section 3.2. Knowing the velocities, the positions of the drops can be advanced according to (6).

3.1. Separated surfaces

When the separation between the interfaces is larger than or comparable with the dimension of the smaller drop, the natural choice is to use the bi-spherical coordinate system (ξ, ζ, ϕ) connected with the two droplets that is linked with the cylindrical system by the following relations: $z = \sinh\xi/h$, $r = \sin\zeta/h$, $h = (\cosh\xi - \cos\zeta)/\sinh\alpha$. The interfaces of the large drop and the small droplet are described by the coordinate surfaces $\xi = \alpha$ and $\xi = \beta$, respectively. If the ratio of the radii R and the separation distance d are given, then α and β can be defined by

$$\cosh\alpha = \frac{(1-R-d)^2 + 1 - R^2}{2(1-R-d)}, \quad \cosh\beta = \frac{1 - R^2 - (1-R-d)^2}{2R(1-R-d)}, \quad 0 < \alpha < \beta. \tag{21}$$

The general solution of the Laplace equation is expressed in the form of Fourier series (see e.g., Subramanian and Balasubramaniam, 2001)

$$c_i = (\cosh\xi - \cos\zeta)^{1/2} \sum_{n=1}^{\infty} U_n(\xi) P_n(\cos\zeta), \quad i = 0, 1, \tag{22}$$

where

$$U_n(\xi) = E_n^i \cosh(n + 1/2)\xi + G_n^i \sinh(n + 1/2)\xi, \tag{23}$$

while $P_n(\mu)$ are Legendre polynomials. Substituting these series into boundary conditions (9)–(11) results in an infinite system of linear algebraic equations for the coefficients E_n^i and G_n^i, which we then solve for a specified level of accuracy (see Golovin et al., 1995 and Appendix A for more details). As soon as the concentration field is available, the stream function can be determined using the algorithm developed for computing the interaction of two drop under Marangoni convection (Morton et al., 1990).

The general solution of (14) in bi-spherical coordinates was given by Stimson and Jeffrey (1926) as

$$\Psi_i = (\cosh\xi - \mu)^{-3/2} \sum_{n=1}^{\infty} W_n^i(\xi) C_{n+1}^{-1/2}(\cos\zeta), \quad i = 0, 1, 2, \tag{24}$$

where $C_{n+1}^{-1/2}$ are the Gegenbauer polynomials and with the general form of the coefficients W_n^i being

$$W_n^i = A_n^i \cosh(n-1/2)\xi + B_n^i \sinh(n-1/2)\xi + C_n^i \cosh(n+3/2)\xi + D_n^i \sinh(n+3/2)\xi \tag{25}$$

Substituting (24) and (25) into boundary conditions (15)–(17) results in a finite system of linear equations for the coefficients of the stream function for any choice of n. The right-hand side of this system depends on the coefficients E_n^i, and F_n^i (see Golovin et al., 1995 and Appendix A for the details). The forces exerted on the drops by the flow can be computed according to (Happel and Brenner, 1965)

$$F_{1,2} = \frac{2\pi\mu_{0,1}\sqrt{2}}{\sinh\alpha} \sum_{n=1}^{\infty} (A_n^{0,1} + B_n^{0,1} + C_n^{0,1} + D_n^{0,1}). \tag{26}$$

3.2. Surfaces at near-contact

The use of bi-spherical coordinates becomes impractical as the separation distance tends to zero due to the slow convergence of the Fourier series (22) and (24). An appropriate method of analysis in this limit relies on the lubrication approximation for the fluid motion inside the narrow gap between the drops, coupled with the thermo-capillary flow established inside and around the contacting pair of bodies (Loewenberg and Davis, 1993). Analysis shows that, when the droplet is close to the interface of the drop, i.e. for small d, the dimensionless hydrodynamic resistance to the relative motion grows as $F_r \simeq d^{-1/2}$.

The thermo-capillary part of the force and the hydrodynamic resistance of two drops moving with equal velocities, denoted as F_i^{m} and F_i in (19) and (20), depend continuously on d and may be approximated with the value at $d = 0$. In this case of touching drops, the force balance should be modified by introducing a 'contact force', F_c, that acts on the droplet and on the outer surface with equal magnitude and opposite direction at the point of their contact. The force balance on the large drop is given by (19), while the force exerted on the inner drop is balanced by the 'contact force', which is given by

$$F_c = F_2^{\mathrm{g}} + F_2^{\mathrm{m}} - \frac{(F_1^{\mathrm{g}} + F_1^{\mathrm{m}})F_2}{F_1}. \tag{27}$$

The velocities of the individual drops at near contact are given by the approximate expressions resulting from the lubrication analysis

$$V_1 = \frac{(F_1^{\mathrm{g}} + F_1^{\mathrm{m}})}{F_1}, \quad V_2 = \mathrm{V}_1 + \mathrm{V}_{\mathrm{r}} = V_1 + \frac{\mathrm{F}_1(\mathrm{F}_2^{\mathrm{g}} + F_2^{\mathrm{m}}) - \mathrm{F}_2(F_1^{\mathrm{g}} + \mathrm{F}_1^{\mathrm{m}}))}{F_{\mathrm{r}}}, \tag{28}$$

The hydrodynamic resistance to the translation of a drop in contact with another drop, F_i, the thermo-capillary part of the force exerted on each drop, F_i^{m}, and the interfacial concentration distribution can be determined via the use of orthogonal tangent-spheres coordinates (ξ, ζ, φ) related to cylindrical coordinates (z, r, φ) by $z = \xi/(\xi^2 + \zeta^2)$, $r = \zeta/(\xi^2 + \zeta^2)$, $h = \xi^2 + \zeta^2$. In this coordinate system the interfaces of the large drop and the small droplet are described by the coordinate surfaces $\xi = \alpha = \frac{1}{2}$ and $\xi = \beta = \frac{1}{2R}$, respectively. The general solution of the Laplace equation is expressed in the form (see e.g. Leshansky et al., 1997)

$$c = (\xi^2 + \zeta^2)^{\frac{1}{2}} \int_0^\infty [H_{0,1}(s) \sinh s\xi + K_{0,1}(s) \cosh s\xi] J_0(s\zeta)\, \mathrm{d}s, \quad \mathbf{x} \in \Omega_{0,1}. \tag{29}$$

Substituting this representation into boundary conditions (9)–(11) results, after certain manipulations, in a system of linear ordinary differential equations and boundary conditions for the functions $H_{0,1}(s)$ and $K_{0,1}(s)$ that can be solved numerically. Note that in a special case of equal diffusivities of the phases, the concentration field is described by the fundamental expression $c = 1/\delta$, were δ is distance from the center of the small sphere and, hence, in this case

$$(\nabla c)_\zeta = \frac{\partial}{\partial \zeta}\left(\frac{1}{\delta(\xi, \zeta)}\right)(\xi^2 + \zeta^2).$$

A general solution of (14) in the domain Ω_1 is (Cooley and O'Neil, 1969)

$$\Psi_1 = \frac{\zeta}{(\xi^2 + \zeta^2)^{\frac{3}{2}}} \int_0^\infty [(A(s) + C(s)\xi) \sinh s\xi + (B(s) + D(s)\xi) \cosh s\xi] J_1(s\zeta)\mathrm{d}s. \tag{30}$$

A solution of (14), bounded in Ω_0 and satisfying conditions (15), is

$$\Psi_0 = \frac{\zeta}{(\xi^2 + \zeta^2)^{\frac{3}{2}}} \int_0^\infty \left[(A_0(s) + C_0(s)\xi)\mathrm{e}^{s\xi} + \frac{1}{2}\mathrm{e}^{-s|\xi|}\left(|\ \xi\ | + \frac{1}{s}\right) V_1\right] J_1(s\zeta)\mathrm{d}s, \tag{31}$$

while a bounded solution for the interior fluid within the small drop, Ω_2, is

$$\Psi_2 = \frac{\zeta}{(\xi^2 + \zeta^2)^{\frac{3}{2}}} \int_0^\infty [(A_2(s) + C_2(s)\xi)\mathrm{e}^{-s\xi}] J_1(s\zeta)\mathrm{d}s, \tag{32}$$

where J_0 and J_1 are Bessel functions of the first kind.

Inserting the stream function expressions into boundary conditions (15)–(17) we obtain a set of algebraic equations to determine the functions $A(s)$, $B(s)$, $C(s)$, $D(s)$, $A_0(s)$, $C_0(s)$, $A_2(s)$ and $C_2(s)$. When these are known, the forces exerted by the flow on each of the drops can be computed according to (18)

$$F_1 = \frac{4\pi}{\mu_1} \int_0^\infty sA_0(s)\mathrm{d}s, \quad \text{and} \quad F_2 = \frac{2\pi\mu_2}{\mu_1} \int_0^\infty s[A(s) + B(s)]\mathrm{d}s. \tag{33}$$

(see Appendix B for more details).

4. Quasi-stationary motion of spherical drops. Results and discussion

4.1. Self-induced motion

We discuss first the case where the motion is driven solely by the Marangoni effect. Our calculations revealed that in the common case when $\sigma_c < 0$, if the drops are not concentric, the inner droplet acquires a velocity directed from the center to the interface of the large drop. The latter drop also begins to move in the same direction. The velocity of the droplet always exceeds that of the drop and the distance between the centers increases. Thus, our results show that the stationary concentric configuration is unstable.

Iso-concentration contours for diffusivity ratio $\kappa = 2$ and $\kappa = 0.2$ ($R = 0.4$, $d = 0.08$) are shown in Fig. 2a and b, respectively. For $\kappa = 1$, iso-concentration lines are circles concentric with the inner droplet. For $\kappa = 0$, the concentration in the outer phase and on the surface of the large drop is uniform and, hence, no Marangoni flow is induced. Streamline patterns for $R = 0.4$, $d = 0.12$, $\kappa = 0.2$, $\mu_1 = \mu_2 = 2$ are shown in the laboratory reference frame in Fig. 3a and in the reference frame linked to the large drop in Fig. 3b. The motion of the two drops in the same direction and the drift of the inner droplet in the direction of the surface of the large one are evident in Fig. 3a and b, respectively. An interesting feature of the motion is the onset of a region of reverse flow (Fig. 3a) similar to that observed by Morton et al. (1990) for a compound drop subjected to an externally imposed temperature gradient. The streamline pattern of the induced flow, shown in Fig. 3b in a frame of reference attached to the large drop, reflects the integral results that the migration velocity of the inner drop is higher than that of the outer drop, and an eventual contact is expected. Typical streamline pattern for two drops moving in contact is illustrated in Fig. 4.

The dependence of the drops' velocities on the diffusivity ratio, viscosity ratio, radii ratio, and interface separation was studied. The results are illustrated in Figs. 5–7. The relative velocity of the drops is depicted in Fig. 5 versus separation distance for various values of the other governing parameters. The velocity vanishes when the drops are concentric and when they touch, and it reaches a maximum value at a certain separation distance that is on the order of the droplet's

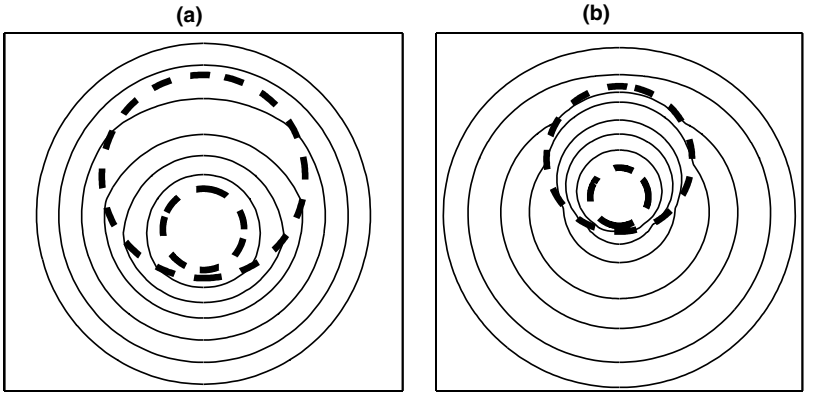

Fig. 2. Iso-concentration contours for $R = 0.4$, $d = 0.08$ (a) $\kappa = 2$, (b) $\kappa = 0.2$. The dashed curves denote the drops' surface.

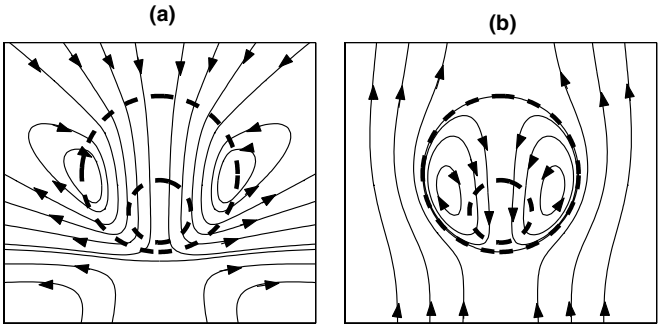

Fig. 3. Streamline patterns for $R = 0.4$, $d = 0.12$, $\kappa = 1$, $\mu_1 = \mu_2 = 2$. (a) Laboratory reference frame. (b) Frame moving with the large drop. The dashed curves denote the drops' surface.

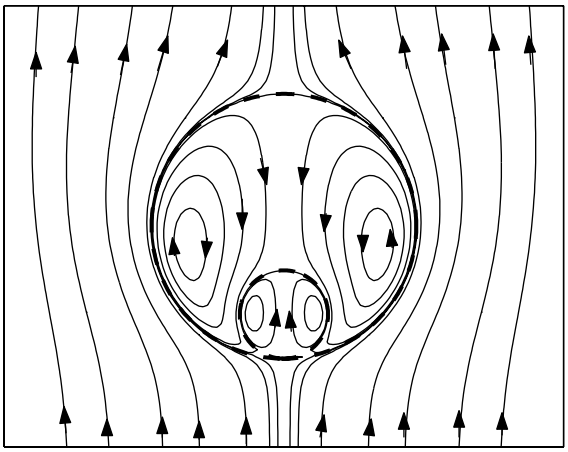

Fig. 4. Streamline patterns for two drops moving in contact, $R = 0.333$, $\kappa = 1$, $\mu_1 = 1$, $\mu_2 = 2$. The reference frame is moving with the aggregate. The dashed curves denote the drops' surface.

radius. A lubrication analysis of the flow at the thin gap between the surfaces, similar to that conducted by Loewenberg and Davis (1993), shows that at small gap thickness d the lubrication resistance is of order $F_r \simeq \mathrm{O}(d^{-1/2})$, which yields that non-deformable drops touch at a finite time. The dependence of the relative velocity on the radii ratio, R, diffusivity ratio, κ and the viscosity ratios, μ_1 and μ_2 are illustrated in Fig. 5a, b, c and d, respectively.

In Fig. 5a, $\mu_1 = \mu_2 = 1$, $\kappa = 1$. Dashed, dashed-dotted, dotted and solid curves correspond to $R = 0.05$, 0.2, 0.5 and 0.75, respectively. The relative velocity decreases with R and vanishes in the limit $R \to 0$ corresponding to vanishing radius of the inner drop. At a fixed separation, the velocity first increases with R, reaches maximum value at $R \simeq 0.5$ and for larger R it decreases.

In Fig. 5b, $\mu_1 = \mu_2 = 1$, $R = 0.2$. Solid, dashed, dotted and dashed-dotted curves correspond to $\kappa = 1$, 2, 10 and 0.2, respectively. The distance, at which the maximum relative velocity is realized, increases with the diffusivity ratio. For a fixed separation, the dependence of the relative velocity on the diffusivity ratio is not monotonic, and it exhibits a maximum at some critical value of κ

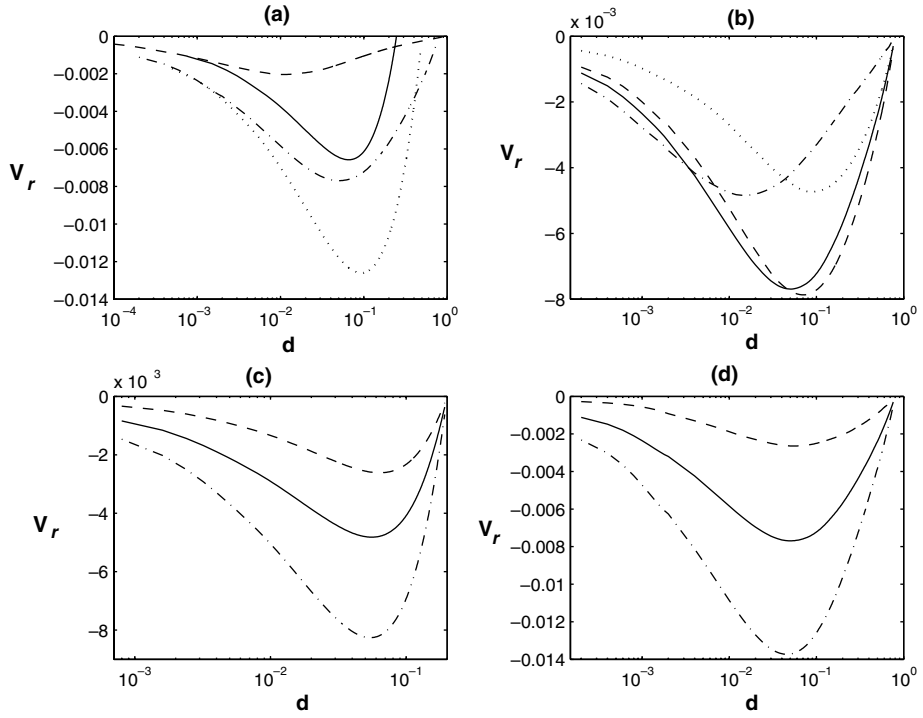

Fig. 5. The inner-sphere relative velocity as a function of the separation between the interfaces. In (a) $\mu_1 = \mu_2 = 1$, $\kappa = 1$. Dashed, dashed-dotted, dotted and solid curves correspond to $R = 0.05$, 0.2, 0.5 and 0.75, respectively. In (b) $\mu_1 = \mu_2 = 1$, $R = 0.2$. Solid, dashed, dotted and dashed-dotted curves correspond to $\kappa = 1$, 2, 10 and 0.2, respectively. In (c) $\kappa = 1$, $R = 0.2$. Solid, dashed and dashed-dotted curves correspond to $\mu_1 = \mu_2 = 1$; $\mu_1 = 10$, $\mu_2 = 0.1$ and $\mu_1 = 0.2$, $\mu_2 = 5$, respectively. In (d) $\mu_2 = 1$, $\kappa = 1$, $R = 0.2$. Solid, dashed and dashed-dotted curves correspond to $\mu_1 = \mu_2 = 1$, 0.2 and 10, respectively.

that decreases with the growth of separation distance. At the limit $\kappa \to 0$, corresponding to the case of non-conducting large drop, the migration velocity vanishes, while at the limit $\kappa \to \infty$ corresponding to the case of non-conducting ambient liquid, the velocity tends to a finite non-zero value.

The dependence of the relative velocity on the viscosity of the inner droplet and on the ambient fluid is illustrated in Fig. 5c and d, respectively. In Fig. 5c $\kappa = 1$ and $R = 0.8$. Solid, dashed and dashed-dotted curves correspond to $\mu_1 = \mu_2 = 1$; $\mu_1 = 10$, $\mu_2 = 0.1$ and $\mu_1 = 0.2$, $\mu_2 = 5$, respectively. In Fig. 5d, $\kappa = 1$, $R = 0.2$. Solid, dashed and dashed-dotted curves correspond to $\mu_1 = \mu_2 = 1$, 0.2 and 10, respectively. One can see that the influence of the viscosity of the droplet on the migration velocity is significant for small separation distances (Fig. 5c), while the growth of the viscosity of the large drop results in a substantial retardation of the motion for any configuration (Fig. 5d).

The velocity of the large drop versus separation distance is shown in Fig. 6. The dependence of the velocity on the radii ratio, diffusivity ratio and the viscosity ratios are illustrated in plots 6a–d, respectively. In Fig. 6a $\mu_1 = \mu_2 = 1$, $\kappa = 1$. Solid, dotted, dashed-dotted and dashed curves

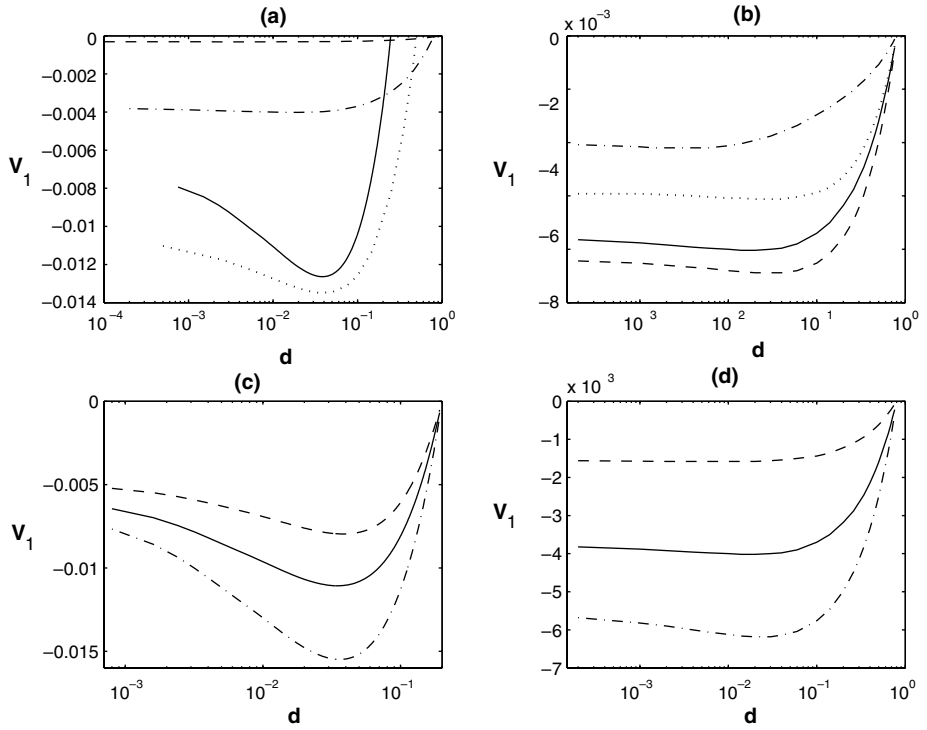

Fig. 6. The outer-sphere velocity as a function of the separation between the interfaces. In (a) $\mu_1 = \mu_2 = 1$, $\kappa = 1$. Solid, dotted, dashed-dotted and dashed curves correspond to $R = 0.75$, 0.5, 0.2 and 0.05, respectively. In (b) $\mu_1 = \mu_2 = 1$, $R = 0.2$. Solid, dashed, dotted and dashed-dotted curves correspond to $\kappa = 1$, 2, 10 and 0.2, respectively. In (c) $\mu_1 = 1$, $\kappa = 1$, $R = 0.2$. Solid, dashed and dashed-dotted curves correspond to $\mu_1 = \mu_2 = 1$; $\mu_1 = 10$, $\mu_2 = 0.1$ and $\mu_1 = 0.2$, $mu_2 = 5$, respectively. In (d) $\kappa = 1$, $R = 0.2$. Solid, dashed, dotted and dashed-dotted curves correspond to $\mu_1 = \mu_2 = 1$, 0.2 and 10, respectively.

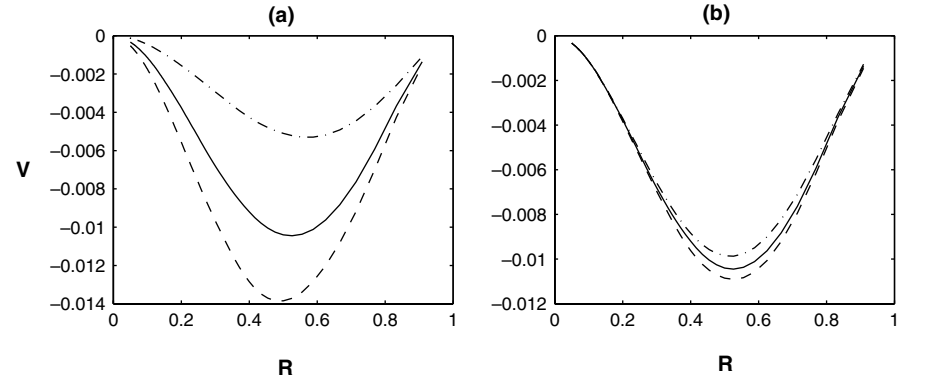

Fig. 7. Velocity of a compound drop with surfaces in contact as function of size ratio. In (a) $\mu_1 = \mu_2$, solid, dashed and dashed-dotted curves correspond to $\mu_1 = 1$, 0.1 and 5, respectively. In (b) $\mu_1 = 1$, solid, dashed and dashed-dotted curves correspond to $\mu_2 = 1$, 0.1 and 5, respectively.

correspond to $R = 0.75$, 0.5, 0.2 and 0.05, respectively. It is evident that the migration velocity grows with the radii ratio and it tends to zero with $R \to 0$. At a fixed separation, the velocity first increases with R, reaches maximum value at $R \simeq 0.5$ and for larger R it decreases.

In Fig. 6b $\mu_1 = \mu_2 = 1$, $R = 0.2$. Solid, dashed, dotted and dashed-dotted curves correspond to $\kappa = 1$, 2, 10 and 0.2, respectively. For large κ, the velocity of the outer drop decays monotonically with the growth of the separation distance, while for smaller κ it exhibits a maximum at some d. For a fixed separation, the dependence on the diffusivity ratio is not monotonic, and it achieves its maximum value at $\kappa \simeq 2$.

In Fig. 6c, $\mu_1 = 1$, $\kappa = 1$, $R = 0.8$. Solid, dashed and dashed-dotted curves correspond to $\mu_1 = \mu_2 = 1$; $\mu_1 = 10$, $\mu_2 = 0.1$ and $\mu_1 = 0.2$, $\mu_2 = 5$, respectively. The velocity of the large drop decays with the growth of the viscosity of the inclusion. The influence of viscosity of the droplet on the migration velocity is pronounced for moderate separations and becomes insignificant when the surfaces come closer. Fig. 6d illustrates the dependence of the aggregate migration velocity on the ratio of its viscosity to that of the ambient medium for $\kappa = 1$, $R = 0.2$. Solid, dashed and dashed-dotted curves correspond to $\mu_1 = \mu_2 = 1$, 0.2 and 10, respectively. The growth of the viscosity of the large drop results in a significant retardation of the motion for any configuration.

From Fig. 6 it is evident that, similar to the relative velocity, the velocity of the larger drop vanishes for the concentric configuration, while when the separation distance tends to zero, the velocity of the large drop tends to a finite non-zero value. Thus, starting from some non-concentric configuration, both drops move in the same direction with the inner droplet having a larger velocity. The eccentricity of the system increases. When the droplet comes closer to the interface of the large drop, its relative motion is retarded by the strong viscous resistance and both particles continue to move with the same speed.

After collision has taken place, the aggregate exhibits steady thermo-capillary migration with the velocity V_1 defined in the first of Eq. (28). Fig. 7 shows the dependence of the migration velocity of the drops pair on the radii ratio R for the particular case of equal diffusivities and for a range of viscosity ratios. In Fig. 7a $\mu_2 = 1$, solid, dashed and dashed-dotted curves correspond to $\mu_1 = 1$, 0.1 and 5, respectively. In Fig. 7b $\mu_1 = 1$, solid, dashed and dashed-dotted curves correspond to $\mu_2 = 1$, 0.1 and 5, respectively. It is evident that the velocity decreases monotonically with the growth of each of the viscosities, with much stronger sensibility to the viscosity of the large drop. Every curve in Fig. 7 exhibits a maximum at $R \simeq 0.5$, and vanishes in the limits $R \to 0$, corresponding to vanishing radius of one of the drops, and $R \to 1$, corresponding to equal-sized drops.

4.2. Combined action of gravity and Marangoni effect

In all the cases discussed thus far in this paper, the flow is driven solely by the Marangoni traction. In many applications, however, gravitational effects also play an important role. In this section we study the combined effect of gravity and thermocapillarity on the motion of a compound drop. We concentrate on the axisymmetric configuration where the centerline of the drops is parallel to the gravity acceleration vector, a case that can be studied using the technique developed in the previous sections. It is anticipated that the axisymmetric configuration is realized in most cases following an initial period during which 3-dimensional flow is present.

Compared to the case of self-induced motion, here the problem has two additional governing parameters, Ar_1 and Ar_2, defined in Section 2, characterizing the relative influence of gravity on the motion of each particle. Note that these parameters may be negative as well as positive. If the averaged density of the aggregate exceeds that of the ambient liquid, the number Ar_1 is negative while in the opposite case it is positive. The other parameter, Ar_2, characterizes the relative influence of buoyancy on the motion of the inner drop.

We do not conduct a full parametric analysis of the problem but rather consider some interesting special cases, where we describe typical flow patterns and give qualitative description of drops behavior.

Some typical dependence of the relative velocity of the two drops (velocity of the droplet in the reference frame attached to the drop) rescaled by the characteristic buoyancy driven velocity of the large drop, V_r/Ar_1, on the center-to-center distance, $Z = Z_2 - Z_1$, are shown in Fig. 8 for a variety of governing parameters. Positive values of Z correspond to the cases when the inner drop is close to the upper surface of the large one. Zero relative velocity corresponds to an equilibrium

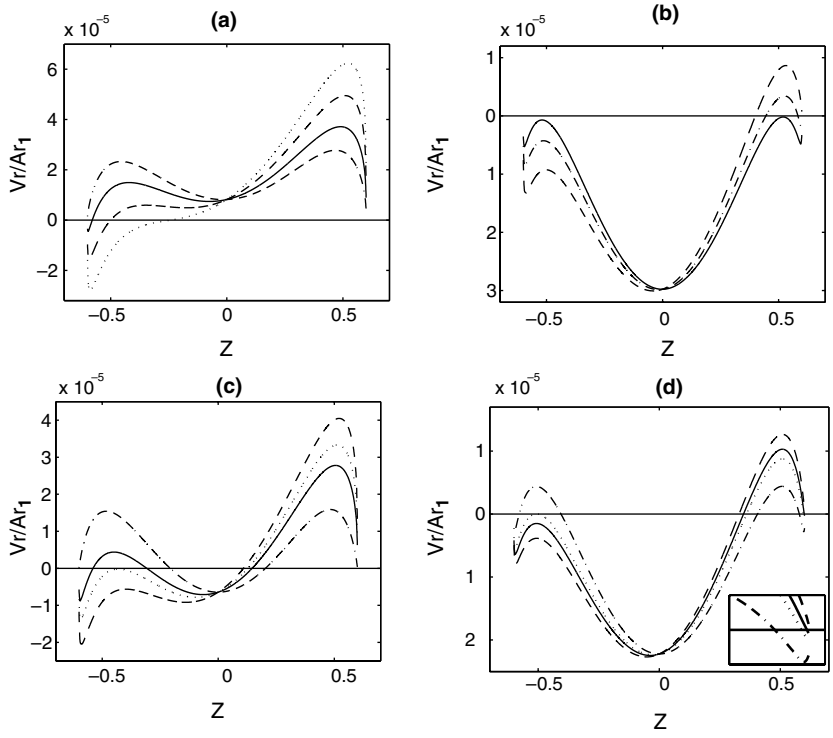

Fig. 8. The inner droplet relative velocity as function of the separation between the centers of the spheres, $R = 0.4$, $\mu_2 = 0$. In (a) $\mu_1 = 10.52$, $Ar_1 = -12.1$ and $Ar_2 = 0$. Dashed, solid, dashed-dotted and dotted lines correspond to $\kappa = 5000$, 1000, 500 and 333, respectively. In (b) $\mu_1 = 9.52$, $Ar_1 = -12.1$ and $Ar_2 = 0.25$. Dashed, solid and dashed-dotted lines correspond to $\kappa = 50000$, 2000 and 833, respectively. In (c) $\mu_1 = 9.7$, $Ar_1 = -12.09$ and $Ar_2 = 0.26$. Dashed, solid, dashed-dotted and dotted lines correspond to $\kappa = 10000$, 1667, 769 and 500, respectively. In (d) $\mu_1 = 9.7$, $Ar_1 = -12.1$ and $Ar_2 = 0.25$. Dashed, solid, dashed-dotted and dotted lines correspond to $\kappa = 10000$, 2867, 2128 and 1485, respectively.

configuration of the system. The velocity is negative in the case of a downward motion (see Fig. 1).

Sadhal and Oguz (1985), studied the buoyancy-driven motion of a compound drop and found that, depending on the governing parameters, there are cases where zero, two or four equilibrium positions of the inner drop inside the outer one exist, in addition to the touching aggregate configuration. Fig. 8 illustrates the combined action of buoyancy and Marangoni effect on the relative motion of a light inner droplet ($Ar_2 > 0$) within the heavy large drop ($Ar_1 < 0$) for $R = 0.4$, $\mu_2 = 0$, and the values of the other parameters corresponding to each of the cases mentioned above.

In Fig. 8a $\mu_1 = 10.53$, $\kappa = 1$ and $Ar_2/Ar_1 = -0.0206$. In the absence of Marangoni effect the internal circulating flow within the large drop is not strong enough to reverse the motion of the droplet. The latter always moves upwards and eventually touches the upper interface. The dashed-dotted curve with $Ar_1 = -12$ illustrates the case of a relatively weak Marangoni effect when the interaction pattern is qualitatively similar to that driven solely by buoyancy. The solid curve is calculated for $Ar_1 = -2450$. Here the Marangoni effect is stronger and results in the appearance of an unstable equilibrium position in the vicinity of the lower interface. The inner droplet released at the position above this equilibrium would move to the upper interface and that released below migrates to the lower interface. With the further increase of Ar_1 this position is shifted upwards (see dashed, $Ar_1 = -1210$ and dotted, $Ar_1 = -80$, lines) and tends to the center of the large drop where it should be located for the motion driven solely by the Marangoni effect.

In Fig. 8b $\mu_1 = 9.524$, $\kappa = 1$, $Ar_2/Ar_1 = -0.0206$. The viscosity of the large drop is lower and the internal circulation is more intensive than in the previous case. In the absence of Marangoni effect the droplet motion within the large drop is always reversed. At any configuration, it moves downwards and eventually touches the lower interface. The dashed line illustrates the case of a weak Marangoni effect and the interaction pattern qualitatively similar to that driven solely by buoyancy. The dashed-dotted curve is calculated for $Ar_1 = -8067$. Here the Marangoni effect is more pronounced and results in the appearance of a pair of equilibrium positions in the upper part of the large drop, with the upper of them being stable. With the further decrease of $|Ar_1|$, the stable position is shifted upwards and eventually merges with the interface of the large drop, as illustrated by the dashed line calculated for $Ar_1 = -1152$. The unstable position is shifted downwards and tends to the center of the large drop where it should by for the motion driven solely by the Marangoni effect.

In Fig. 8c $\mu_1 = 9.7$ $\kappa = 1$, $Ar_2/Ar_1 = -0.0206$. In the absence of Marangoni effect the buoyancy of the droplet is almost compensated by the action of the circulating flow. The direction of its relative motion depends on its position within the large drop. There exist two equilibrium positions of the inner drop within the large one, the lower of them being stable. After being released at a position lower than the unstable equilibrium position the drop would move towards the stable equilibrium, while after release above this critical position it would move to the upper interface. The dashed-dotted curve is calculated for $Ar_1 = -12{,}090$, when the Marangoni effect is relatively very weak, and the curve is similar to that observed for the motion driven solely by buoyancy. The solid line corresponds to $Ar_1 = -2418$. Here the influence of thermocapillarity is evident. The stable equilibrium position is shifted downwards and another unstable equilibrium appears near the lower interface. With the further decrease of $|Ar_1|$, the lower unstable position moves upwards, while the stable one downwards. For $Ar_1 = -1680$ (dotted line) they merge into one unstable

position and for smaller $|Ar_1|$, the interaction pattern is similar to that observed for the motion induced solely by the Marangoni effect when there exists a single equilibrium position of the droplet inside the drop. It is illustrated by dotted line ($Ar_1 = -1209$).

In Fig. 8d $\mu_1 = 9.7$, $\kappa = 2128$, $Ar_2/Ar_1 = -0.0206$. In the absence of Marangoni effect such a pair of drops has four equilibrium positions of the inner drop within the large one, two of them being stable. After being released below the first lower unstable equilibrium position the drop would move downwards and eventually touch the lower interface. An inner drop initially placed between two unstable equilibrium positions migrates toward the lower stable configuration and the drop with the initial position higher than the upper unstable equilibrium migrates to the upper stable equilibrium position. The dashed-dotted curve calculated for $Ar_1 = -10^5$ demonstrates a similar behavior. The dotted curve ($Ar_1 = -16.4$) is already deformed by the Marangoni effect. The two lower equilibrium points merge and only one stable equilibrium in the vicinity of the upper interface is possible. With the further decrease of $|Ar_1|$this equilibrium point is shifted upwards as it is demonstrated by the dotted curve ($Ar_1 = -12.1$) and eventually merges with the upper interface. For smaller $|Ar_1|$the interaction pattern is qualitatively similar to that observed for the motion induced solely by the Marangoni effect as it is shown by the dashed-dotted curve calculated for $Ar_1 = -8.6$.

An interesting sample of the dependence of the velocity of the large drop on the position of the droplet is depicted in Fig. 9 for $R = 0.4$, $\mu_1 = \mu_2 = 1$, $Ar_1 = -0.03625$, $Ar_2 = 0.12$. Dashed, solid and dashed-dotted curves are calculated for $\kappa = 500$, 250 and 160, respectively. The average density of the compound drop exceeds that of the ambient fluid and, when driven solely by buoyancy, it would move downwards for any configuration. The Marangoni effect results in the acceleration of this motion when the inner drop is located below the center of the large one, and in a retardation in the opposite case. When the thermocapillary force is relatively strong, this retardation may lead to the reversal of the motion of the large drop as it is demonstrated by the solid and dashed-

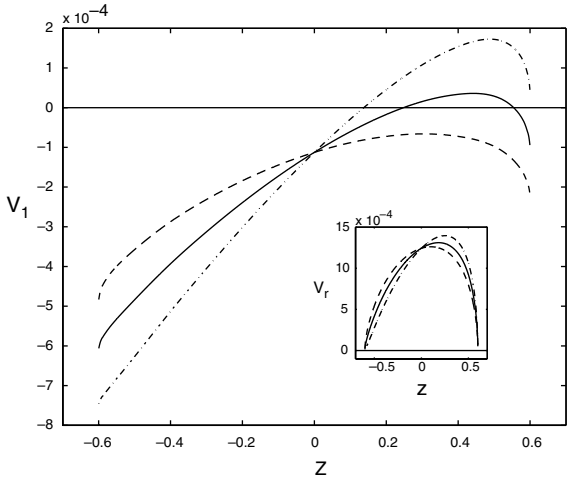

Fig. 9. The outer drop velocity as function of the separation between the centers of the spheres. In (a) $\mu_1 = \mu_2 = 1$, $\kappa = 1$, $Ar_1 = -0.03625$ and $Ar_2 = -0.12$. Dashed, solid and dashed-dotted curves correspond to $\kappa = 500$, 250 and 160, respectively.

dotted curves. The relative velocity of the inner drop in these cases is directed upwards. If initially the droplet was placed below the large drop center, then in all the cases the compound drop first moves downwards and, in the case of a weak Marangoni effect, the motion maintains its direction (see the dashed curve). In contrast to this, for smaller values of Ar the motion of the large drop is reversed when the inner droplet reaches some critical position inside it. The aggregate migrates upwards and the inner drop continues to approach the upper interface. For strong enough thermocapillarity, the upward motion is kept afterwards (see the dashed-dotted curve), while for intermediate values of κ, the motion is reversed once more when the inclusion reaches the second critical position shown by the solid curve.

As it was shown above, the competition between buoyancy and the Marangoni flow induced on the surface of the large drop results in complex combinations of the direction of motion of two particles. In Figs. 10–12 we present a sample collection of flow patterns and streamlines for a few of these possible realizations that depend on the combination of physical parameters and the position of the small drop within the large one. The streamline patterns are depicted in the laboratory reference frame. In all the cases $\mu_1 = \mu_2 = \kappa = 1$, $R = 0.2$. In Fig. 10a $d = 0.46$, $Ar_1 = -0.587$, $Ar_2 = 1.038$. The large drop moves upwards while the small one downwards.

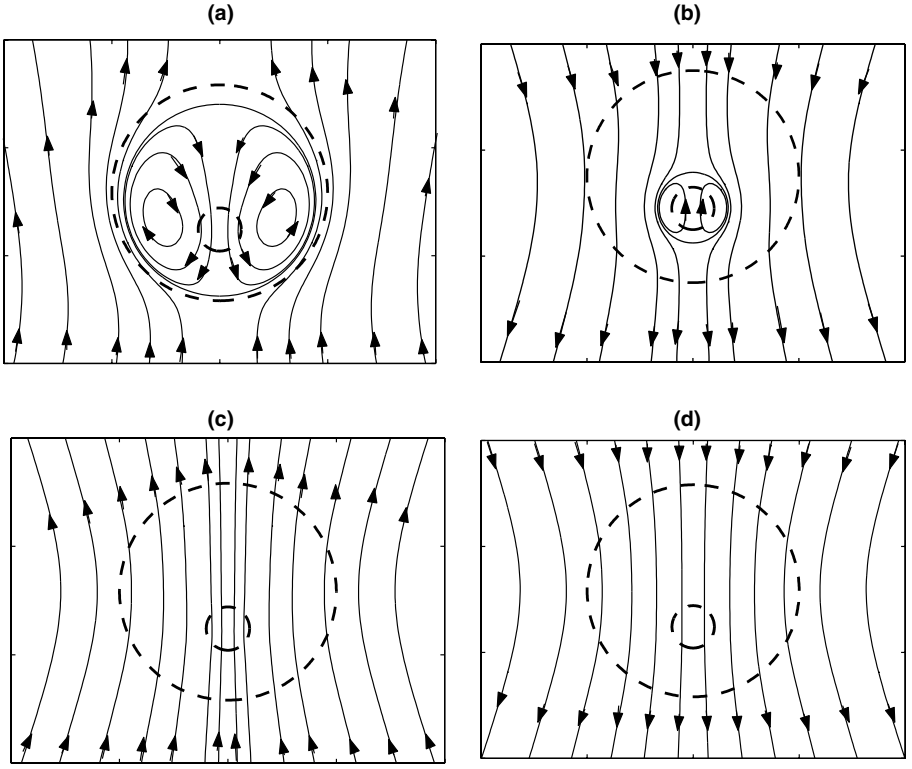

Fig. 10. Streamline patterns with combined action of gravity and Marangoni effect. $R = 0.2$, $\mu_1 = \mu_2 = \kappa = 1$. In (a) $d = 0.46$, $Ar_1 = -0.587$, and $Ar_2 = 1.038$. The large drop moves upwards while the small one downwards. In (b) $d = 0.5$, $Ar_1 = 5.19$, $Ar_2 = -7.785$. The larger drop moves downwards while the small one upwards. In (c) $d = 0.46$, $Ar_1 = 5$, $Ar_2 = 67.5$. Both particles move upwards. In (d) $d = 0.46$, $Ar_1 = -0.5$, $Ar_2 = -63$. Both particles move downwards.

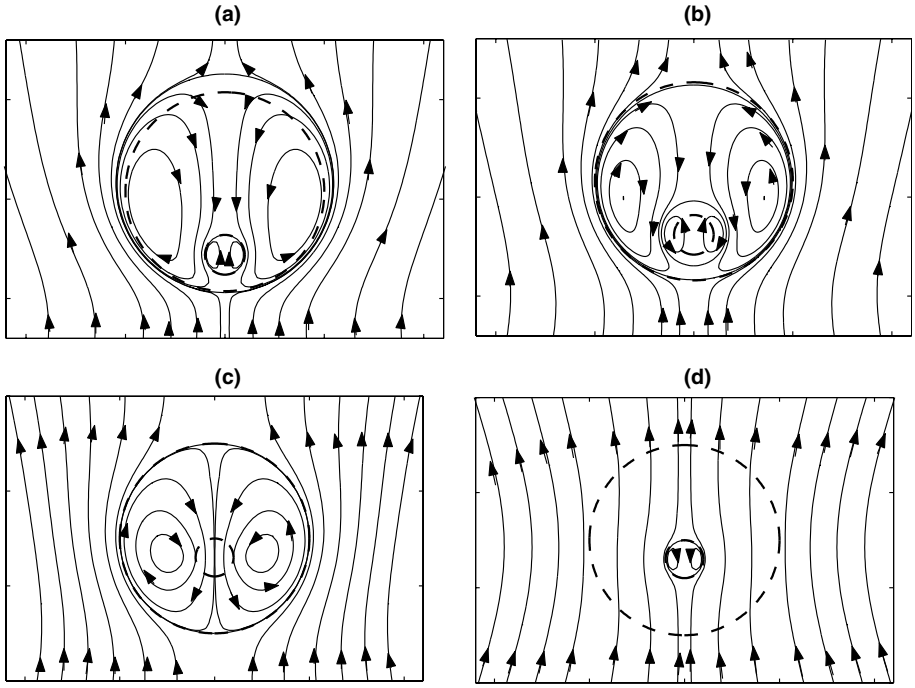

Fig. 11. Streamline patterns with combined action of gravity and Marangoni effect. $R = 0.2$, $\mu_1 = \mu_2 = 1$, $\kappa = 1$. In (a) $h = 0.166$, $Ar_1 = Ar_2 = 1$. In (b) $d = 0.26$, $Ar_1 = Ar_2 = 1$. In (c) $d = 0.6$, $Ar_1 = -2.158$, $Ar_2 = 0.917$. In (d) $d = 0.6$, $Ar_1 = -1.268$, $Ar_2 = 4.659$.

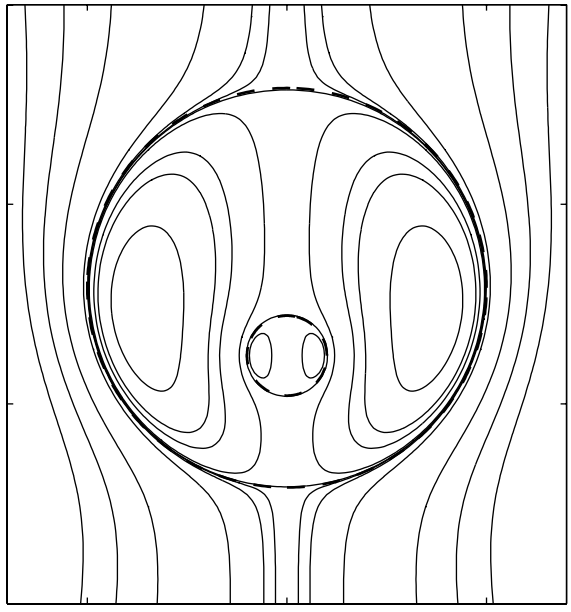

Fig. 12. Streamline pattern for the case where the two bodies remain motionless. $R = 0.2$, $\mu_1 = \mu_2 = \kappa = 1$, $d = 0.46$, $Ar_1 = -0.286$, $Ar_2 = 0.661$.

The opposite case, where the larger drop moves downwards while the small one upwards, is illustrated in Fig. 10b where $d = 0.5$, $Ar_1 = 5.19$, $Ar_2 = -7.785$. Note the separation streamline within the large drop. The streamline patterns in the cases when the drops move in the same direction, upwards or downwards, are illustrated in Fig. 10c and d.

We notice that there exist dynamic cases for which one of the drops is immobile in the laboratory frame although all fluids in the bulks and at the surfaces are circulating. Some of such cases are illustrated in Fig. 11. In Fig. 11a $d = 0.166$, $Ar_1 = Ar_2 = 1$. Both drops are buoyant and would move upwards in the absence of Marangoni effect. Thermocapillarity results in a downward migration of the large drop and immobilization of the small one. A closed separation streamline is evident in outer fluid around the large drop. In Fig. 11b, $d = 0.26$, $Ar_1 = Ar_2 = 1$. Here the small drop is closer to the center of the large one and the influence of the Marangoni effect is weaker than in the previous case. The large drop is quiescent while the small one drifts upwards. The separation line is evident inside the large drop around the small one. In Fig. 11c, $d = 0.46$, $Ar_1 = -2.158$, $Ar_2 = 0.917$. The density of the large drop is higher than that of the ambient medium, while the density of the droplet is lower. The Marangoni force that is directed downwards makes the small particle move against buoyancy, while the large one remains immobile. The separation streamline coincides with the interface of the drop. In Fig. 11d, $d = 0.46$, $Ar_1 = -1.268$, $Ar_2 = 4.659$. A separation streamline is evident in the outer fluid near the drop's interface.

For a certain values of parameters the Marangoni effect may compensate the buoyancy forces acting on both drops and result in stationary configuration of neutrally buoyant particles. An example for the streamline pattern in such a case is illustrated in Fig. 12 ($d = 0.46$, $Ar_1 = -0.286$, $Ar_2 = 0.661$), where it is evident that all fluids are circulating and the surfaces of both drops are stream surfaces.

5. Unsteady and convective mass transfer

In this section we study the case when convective transport effects should be taken into account while inertia is still negligible. When the Peclet number is non-zero, the convective term in (7) couples hydrodynamics and species transport. For small Pe, it is reasonable to anticipate that the solution will be close to the quasi-steady one discussed above, and search for a small correction. Below we construct a leading order correction term following Lavrenteva et al. (1999) and Leshansky et al. (2001). Our study of non-stationary convection transport at high Peclet in a special case when the resistance to mass transfer is concentrated mostly in the ambient fluid is performed following the methods of Lavrenteva and Nir (2001).

5.1. Low Peclet number corrections

At zero Pe, the concentration field, $c(t,\mathbf{x})$, is a harmonic function in Ω_0 exhibiting the asymptotic behavior

$$c(t,\mathbf{x}) = a(t)/|\mathbf{x}| + \mathrm{O}(1/|\mathbf{x}|^2) \tag{34}$$

at $|\mathbf{x}| \to \infty$. For non-zero Pe we consider the case when it is of the same order of magnitude in the various phases. An attempt to make use of regular perturbation techniques results, for the leading

order correction term, in a Poisson equation with the right-hand-side that decays as $1/|\mathbf{x}|$at large $|\mathbf{x}|$, which does not admit a solution decaying at infinity. The failure of regular perturbations expansion underscores the need for singular perturbations.

Following the well-established procedure of matched asymptotic expansions (see e.g. Van Dyke, 1975), inner expansion

$$c(t,\mathbf{x}) = c^0(t,\mathbf{x}) + \sum_{n=1}^{\infty} f_{\text{in}}^n(\varepsilon) c^n(t,\mathbf{x}), \tag{35}$$

and outer expansion

$$H(t,\xi) = \sum_{n=0}^{\infty} f_{\text{out}}^n(\varepsilon) H^n(t,\boldsymbol{\xi}), \quad \xi = \varepsilon\mathbf{x}, \tag{36}$$

of the concentration field are introduced and then matched to satisfy appropriate conditions. The inner expansion satisfies the required conditions on the interfaces, while outer expansion decays at infinity.

At low Reynolds numbers, the velocity and associated pressure fields satisfy stationary Stokes equations, which do not contain a small parameter. The solution is on the order of the concentration and may be expanded in a regular perturbation series with coefficients that depend on ε in a manner that is similar to that displayed in the inner expansion for the concentration. Similar expansions are anticipated for the drop velocities (see Lavrenteva et al., 2002 for more details).

Substituting expressions (35) and (36) into the governing equations and matching conditions, we find that $\varepsilon = Pe^{1/2}$, $f_{\text{out}}^0 = f_{\text{in}}^1 = \varepsilon$. The drops velocities are given by

$$V_i = V_i^0 + \varepsilon V_i^1 + \mathrm{O}(\varepsilon^2), \tag{37}$$

where V_i^0 is the velocity obtained by setting $Pe = 0$,

$$V_i^1 = \frac{V_i^{0,0}}{\sqrt{\pi}} \int \frac{\mathrm{d}a}{\mathrm{d}t} \frac{\mathrm{d}\tau}{\sqrt{t-\tau}} \tag{38}$$

with $V_i^{0,0}$ being the velocity of the self-induced motion at a given geometry (i.e. in the absence of gravity).

Thus, the leading order correction to the quasi-steady solution appears in the form of a Basset-type history term of $\mathrm{O}(Pe^{1/2})$. This term describes the inherent unsteadiness of the process due to the temporal changes in the relative position of the inner drop, and is important during the transient period. As the inner drop approaches its stable stationary position, the leading order correction is downgraded to $\mathrm{O}(Pe)$. Samples of the temporal dependences of $V_r^1 = V_2^1 - V_1^1$ for $R = 0.2$, $\mu_1 = \mu_2 = 1$ are illustrated in Fig. 13. The dashed and solid lines correspond to the initial separations $d_0 = 0.6$ and 0.4, respectively. The upper lines are calculated for $\kappa = 2$, while the lower ones for $\kappa = 0.84$. Note that the quasi-stationary relative velocities are negative (separation decreases with time) in all four cases. Hence, the convective transfer induced corrections lead to the increase of the relative velocity for $\kappa < 1$ and to its decrease for $\kappa > 1$. In all the cases the absolute value of the correction first grows, then decays and vanishes as the inner drop touches the interface of the larger one and in which case the geometry of the system becomes stationary.

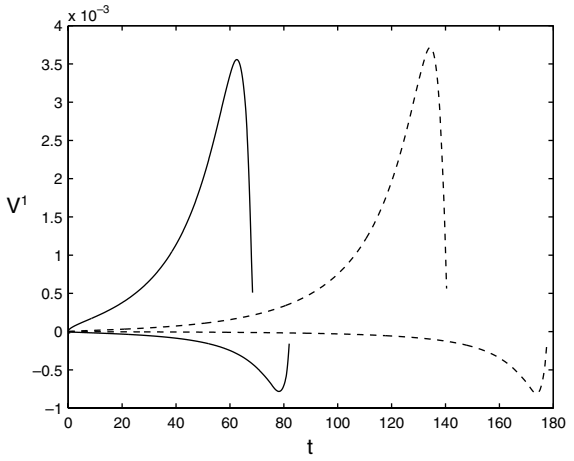

Fig. 13. Sample of the dependence on time of the correction to the relative velocity V_r^1 due to convective mass transfer at low Peclet number. $R = 0.2$, $\mu_1 = \mu_2 = 1$. Dashed and solid lines correspond to $d_0 = 0.6$ and $d_0 = 0.4$, respectively. Upper lines are calculated for $\kappa = 2$, while lower ones for $\kappa = 0.84$.

5.2. Convective effects at high Peclet number

Consider the case $Pe_1 \ll \mathrm{O}(1) \ll Pe_0 = Pe$, when the resistance to mass transfer is concentrated mostly in the ambient fluid (see Lavrenteva and Nir, 2001 for a detailed analysis). To a first approximation at $t \leqslant \mathrm{O}(Pe_0)$, the concentration in the outer medium remains equal to its initial value, $c_0 = 0$. Inside the drop, the leading-order approximation of the concentration satisfies Laplace equation with the boundary conditions.

$$c_1 = 0 \quad \text{at } \mathbf{x} \in \partial\Omega_0, \quad c_1 = 1 \quad \text{at } \mathbf{x} \in \partial\Omega_2. \tag{39}$$

The zero-order solution in $\mathbf{R}^3$, determined as $c^0 = \{c_i, \mathbf{x} \in \Omega_i, i = 0,1\}$ does not satisfy the mass flux balance condition on the interface $\partial\Omega_0$ and thus an external concentration boundary layer should be considered along this surface.

Note that it follows from (39) that to this order the interfacial concentration remains uniform and no Marangoni motion occurs. Hence the zero-order term in the expansion of the stream function equals zero and the first-order term in the concentration expansion in the continuous phase satisfies a time-dependent diffusion equation without convective terms. Introduction of the stretched boundary layer variables, $Y = (r-1)/\varepsilon$ and $c = (c^0-1)/\varepsilon$, $\varepsilon = Pe^{-1/2}$, into this equation and the initial and boundary conditions results in the following boundary value problem:

$$\frac{\partial c}{\partial t} = \frac{\partial^2 c}{\partial Y^2}, \quad Y > 0, \tag{40}$$

subject to

$$\frac{\partial c}{\partial Y} = \phi(t,\theta) = \frac{1}{\kappa}\frac{\partial c_1^0}{\partial r}, \quad Y = 0 \tag{41}$$

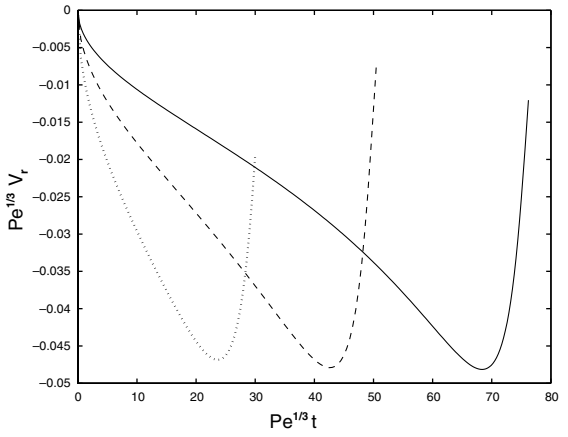

Fig. 14. Sample of the dependence on time of the scaled relative velocities where $R = 0.2$, $\mu_1 = \mu_2 = 1$, $\kappa = 1$. Solid, dashed and dotted curves correspond to initial separations $d_0 = 0.4$, 0.3 and 0.1.

and $c = 0$ at $t = 0$. θ is an angle measured from the axis of symmetry. The specified initial boundary value problem has a unique solution, which on the interface $Y = 0$ reduces to

$$c(t,0,\theta) = \frac{1}{\sqrt{\pi}} \int \frac{\phi(\tau,\theta)}{\sqrt{t-\tau}} \mathrm{d}\tau. \tag{42}$$

As soon as the distribution of the surfactant along the interface is known, the Marangoni flow and the drift velocities of the drops which are linear operators on the $\partial c(t,0,\theta)/\partial\theta$ can be evaluated. An analysis of the equation of motion similar to that of Lavrenteva and Nir (2001) leads to the conclusion that the characteristic transient period before the drops' interfaces touch is in this case of $\mathrm{O}(Pe^{1/3})$. Samples of temporal dependence of the scaled relative velocities are shown in Fig. 14 where $R = 0.2$, $\mu_1 = \mu_2 = 1$, $\kappa = 1$. Solid, dashed and dotted curves correspond to the initial separations $d_0 = 0.4$, 0.3 and 0.1, respectively. In all the cases the velocity first grows and then decays as the inner drop approaches the interface of the lager one.

6. Deformable interfaces

If the capillary numbers are small, $Ca_2 \sim Ca_1 = \varepsilon \ll 1$, it is natural to assume that the deformations of the interfaces are small and to construct solutions of (1)–(9) making use of regular perturbation techniques. Following the derivation of Berejnov et al. (2002) we describe the interfaces using two separate polar coordinates, r_i, θ_i, φ, with origins at the centers of the undeformed drops, $r_i = R_i(\theta_i)$. An alternative approach based on the bi-spherical coordinates was developed in Chervenivanova and Zapryanov (1989). We construct a solution in the form of simple asymptotic expansions in terms of powers of ε in which

$$p_0 = p_0^0 + \varepsilon p_0^1 + \cdots, \quad p_1 = \frac{2}{\varepsilon} + p_1^0 + \varepsilon p_1^1 + \cdots, \quad p_2 = \frac{2}{\varepsilon}\frac{Ca_1}{Ca_2} + p_2^0 + \varepsilon p_1^1 + \cdots,$$

$$\mathbf{V}_i = \mathbf{V}_i^0 + \varepsilon \mathbf{V}_i^1 + \cdots, \quad R_i(\theta_i) = R_i + \varepsilon f_i(\cos(\theta_i)) + \cdots, \quad i = 1, 2,$$

$$c = c^0 + \varepsilon c^1 + \cdots, \quad \mathbf{v}_i = \mathbf{v}_i^0 + \varepsilon \mathbf{v}_i^1 + \cdots, \quad i = 0, 1, 2.$$

Substituting these expansions into Eqs. (1)–(9) gives, at the leading order, the problem that coincides with the problem for non-deformable drops solved in Sections 3 and 4. The normal stress balance in Eq. (4), to within terms of $O(\varepsilon)$, takes the form

$$\frac{\mathrm{d}}{\mathrm{d}\mu_i}\left[(1-\mu_i^2)\frac{\mathrm{d}f_i}{\mathrm{d}\mu_i}\right] + 2f_i = Q_i(\mu_i) + b_i, \quad i = 1, 2, \tag{43}$$

where

$$Q_i(\mu_i) = 2R_i c^0 - R_i^2[\mathbf{n}\cdot\mathbf{\Pi}^0\cdot\mathbf{n}],$$

$\mu_i = \cos\theta_i$ and $[\mathbf{n}\cdot\mathbf{\Pi}^0\cdot\mathbf{n}]$ denotes the jump of the normal stresses across the interfaces evaluated at the unperturbed boundaries. The appearance of the dimensionless constants b_i reflects the fact that the pressure inside the drops can be found up to an additive constant in excess of the static values $2\sigma/a_i$. These constants can be found from the requirement of the incompressibility of the drops.

The homogeneous solutions of (43) are $s_1(\mu) = \mu$ and $s_2(\mu) = F(-1/2, 1, 1/2, \mu^2)$, with F being the hypergeometric function. Note, that s_2 has logarithmic singularities at $\mu = \pm 1$. The complete bounded solution of (43) can be written as

$$f_i = \left[\mu_i \int_{-1}^{\mu_i} Q_i(\mu) s_2(\mu)\mathrm{d}\mu + s_2(\mu_i)\int_{-1}^{\mu_i} Q_i(\mu)\mu\mathrm{d}\mu + b_i + c_i^1\mu_i\right]. \tag{44}$$

The constants b_1 and b_2 are to be found from the condition that the volume of each drop remains unchanged

$$\int_{-1}^{1} f_i(\mu)\mathrm{d}\mu = 0.$$

The terms proportional to μ_i correspond to the displacement of the drops retaining their spherical form.

The results of numerical solutions for the perturbations of the shape of the drops are presented schematically in Fig. 15. It should be noted that, as can be expected, the deformations are negligibly small. Hence, we used $O(1)$ values of Ca to make the small deformations visible. The case of spontaneous motion is illustrated in Fig. 15a. The inner and the outer drops are, respectively, of the form of prolate and oblate spheroids, with higher deformations in the near-contact region. In the case of combined action of gravity and thermocapillarity we illustrate a special case of equilibrium drops (see Fig. 15b). Here, the inner drop has an oblate form, while the outer is prolate. Magnitude of deformations increase with the approach of the interfaces.

The above analysis is valid when the separation distance is much larger than the magnitude of deformations. When the interfaces come closer, the analysis should be modified. The problem can be solved by matched asymptotic expansions for small Ca following e.g. Yiantsios and Davis (1990). This is beyond the scope of the present paper, but by the analogy with the case of two

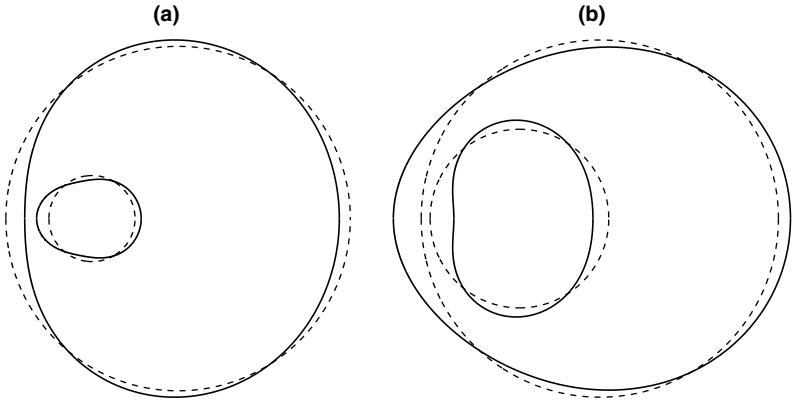

Fig. 15. Small deformations of the drops. (a) spontaneous motion. (b) equilibrium under combined action of gravity and Marangoni effect. The dashed curves denote the unperturbed drops' surfaces.

drops case, it can be anticipated that the deformability will prevent interface touching in finite time.

7. Conclusions

The internal secretion of a weak surface-active substance from the inner droplet induces the locomotion of a compound viscous drop. It was found that although the surface of the inner droplet has a uniform concentration, the Marangoni flow generated around the surface of the large drop causes its center to drift in the direction of the enclosed droplet. The flow generated by the interface of the large drop causes the migration of the internal droplet in the same direction, and an external separated reverse flow appears. In general it was found that the velocity of the inner droplet exceeds that of the large drop. With the passage of time, the droplet approaches the interface of the drop and the eccentricity of the system is increased. When the distance between the centers increases, the relative velocity first grows, but when the droplet approaches to the interface, its relative motion is retarded by the strong viscous resistance. At the limiting configuration of the touching droplets the aggregate will move with a constant velocity.

The combined effect of the buoyancy and spontaneous Marangoni motion is studied as well. It is shown that a rich variety of interaction patterns may occur, which exhibits separation of flow in the outer fluid and within the large drop. In some particular cases both drops remain suspended motionless in the laboratory reference frame with the fluid circulating in a steady manner. A pair of drops may have several equilibrium positions, with one or two of them being stable.

In all the cases, after a transient period of unsteady motion, the system reaches a steady configuration. For the self-induced motion, the equilibrium position of the inner drop is either concentric or touching the interface of the large drop. In the case of combined action of buoyancy and thermocappilarity, eccentric equilibrium configurations are possible as well. Thermocapillary effect does not vanish at an equilibrium state, unless the drops are concentric, and induces an $O(1)$ contribution to the steady migration velocity.

Our main results are calculated for the simplified case of non-deforming surfaces and neglecting inertia, and when diffusion dominates the mass transfer mechanisms in the bulks. The effect of inertia was estimated as $O(Re)$ for the transient period and $O(Re^2)$ for the stationary state, being thus negligibly weak for the low Re flows under consideration. The effect of small but non-zero convective transport was shown to be of $O(Pe^{1/2})$ during the unsteady transient period and to reduce to $O(Pe)$ as the stationary state is established. For another limiting case of high Peclet number of the ambient phase, it was demonstrated that the self-induced motion is slow and an $O(1)$ displacement of the drops occurs in time $O(Pe^{-1/3})$. The evolution of the migration velocities was calculated for a variety of governing parameters. Deformations of the drops surfaces for low capillary numbers were shown to be of $O(Ca)$. Calculations performed for sample cases revealed nearly spheroidal, either oblate or prolate, shapes of perturbed interfaces with higher deformations in the gap region.

Acknowledgment

The research was supported by ISF grant 74/01. DTs and OML acknowledge the support of the Israel Ministry for Immigrant Absorption.

Appendix A. Bi-spherical coordinates

Substituting series representation (22) into the boundary conditions (9)–(11) results in the following infinite system of linear algebraic equations:

$$E_n^0 = G_n^0, \tag{A.1}$$

$$E_n^1 \cosh(n+1/2)\beta + G_n^1 \sinh(n+1/2)\beta = \sqrt{2}\mathrm{e}^{-(n+1/2)\beta}, \tag{A.2}$$

$$(E_n^1 - E_n^0)\cosh(n+1/2)\alpha + (G_n^1 - G_n^0)\sinh(n+1/2)\alpha = 0, \tag{A.3}$$

$$\begin{aligned} E_n^0 \mathrm{e}^{(n+1/2)\alpha} &+ \frac{(2n+1)\coth\alpha}{\kappa-1}\left[(\kappa E_n^1 - E_n^0)\sinh(n+1/2)\alpha + (\kappa G_n^1 - G_n^0)\cosh(n+1/2)\alpha\right] \\ &= \frac{n}{(\kappa-1)\sinh\alpha}\left[(\kappa E_{n-1}^1 - E_{n-1}^0)\sinh(n-1/2)\alpha + (\kappa G_{n-1}^1 - G_{n-1}^0)\cosh(n-1/2)\alpha\right] \\ &\quad + \frac{n+1}{(\kappa-1)\sinh\alpha}\left[(\kappa E_{n+1}^1 - E_{n+1}^0)\sinh(n+3/2)\alpha + (\kappa G_{n+1}^1 - G_{n+1}^0)\cosh(n+3/2)\alpha\right]. \end{aligned} \tag{A.4}$$

To solve this system numerically, we can fix numbers of terms, for example N, and assume $E_n = 0$ for $n > N$. By solving the resulting finite system, the coefficients $E_1^0, E_2^0, \ldots, E_N^0$,

$E_1^1,\ E_2^1,\ldots,\ E_N^1;\ G_1^0,\ G_2^0,\ldots,\ G_N^0;\ G_1^1,\ G_2^1,\ldots,\ G_N^1$ can be found. Increasing the number N, the solution can be found with a desired accuracy.

As soon as the concentration field is available, the stream function can be determined in the form (24) and (25). Substituting (24) and (25) into boundary conditions (15)–(17), where the tangential component of the viscous stress tensor, used in (16) and (17) are of the form

$$\Pi_{\xi\zeta} = h\left(\frac{\partial U_\xi}{\partial\zeta} + \frac{\partial U_\zeta}{\partial\xi}\right) + \frac{1}{\sinh\alpha}(U_\zeta \sin\xi + U_\xi \sin\zeta)$$

results in the following finite system of linear equations on the coefficients of stream function at any n. The right-hand side of this system depends on the coefficients E_n^i and F_n^i (Golovin et al., 1995)

$$A_n^2 = -B_n^2, \quad A_n^0 = B_n^0, \quad C_n^0 = D_n^0, \quad C_n^0 = -D_n^0, \tag{A.5}$$

$$W_n^2(\alpha) = W_n^1(\alpha) = -\frac{(n+1)nV_1\sinh^2\alpha\sqrt{2}}{2}\left(\frac{e^{-(n-1/2)\alpha}}{2n-1} - \frac{e^{-(n+3/2)\alpha}}{2n+3}\right), \tag{A.6}$$

$$W_n^2(\beta) = W_n^1(\beta) = -\frac{(n+1)nV_2\sinh^2\alpha\sqrt{2}}{2}\left(\frac{e^{-(n-1/2)\beta}}{2n-1} - \frac{e^{-(n+3/2)\beta}}{2n+3}\right), \tag{A.7}$$

$$\frac{dW_n^2(\xi)}{d\xi} - \frac{dW_n^1(\xi)}{d\xi} = 0, \xi = \alpha, \beta, \tag{A.8}$$

$$\mu_1\frac{d^2W_n^1}{d\xi^2} - \mu_2\frac{d^2W_n^2}{d\xi^2} = \frac{(n+1)n(2n+1)\sqrt{2}}{4}(\mu_1-\mu_2)V_2\sinh^2\alpha e^{-(1+1/2)\beta}\left(\frac{2\cosh\beta}{2n+1} - \sinh\beta\right), \tag{A.9}$$

$$\frac{d^2W_n^0}{d\xi^2} - \mu_1\frac{d^2W_n^1}{d\xi^2} = \frac{(n+1)n(2n+1)}{2}\left[\int_{-1}^{1}\frac{C_{n+1}^{-1/2}(\mu)}{(\cosh\xi-\mu)^{1/2}}\frac{\partial\gamma}{\partial\mu}d\mu + \frac{\sqrt{2}}{2}(1-\mu_1)V_1\sinh^2\alpha e^{-(1+1/2)\alpha}\left(\frac{2\cosh\alpha}{2n+1} - \sinh\alpha\right)\right]. \tag{A.10}$$

Substitution (25) for W_n^i yield system of eight linear equations for the eight unknown coefficients $A_n^i,\ B_n^i,\ C_n^i,\ D_n^i,\ i = 0, 1, 2$.

An integral term in the right-hand side of (A.10) was calculated according to

$$\int_{-1}^{1}\frac{C_{n+1}^{-1/2}(\mu)}{\cosh(\xi-\mu)^2}\frac{\partial\gamma}{\partial\mu}d\mu = \frac{2U_n(\xi)}{2n+1} - \frac{1}{2}\sum_{j=1}^{\infty}U_n(\xi)\int_{-1}^{1}\frac{P_j(\mu)C_{n+1}(\mu)}{\cosh\xi-\mu}d\mu.$$

Appendix B. Tangent-sphere coordinates

Substituting representation (29) into boundary conditions (10), (11) and the requirement of the continuity of c at the boundary of the large drop leads to the following linear relations between the functions $H_0(s)$, $K_0(s)$, $H_1(s)$ and $K_1(s)$,

$$H_0 = 0,\ K_1(s) = -H_1(s)\tanh\beta s + \frac{2}{1+\mathrm{e}^{2\beta s}},\ K_0(s) - K_1(s) = H_1(s)\tanh\alpha s. \tag{B.1}$$

The concentration field, thus, takes the form

$$\begin{aligned} c &= (\xi^2+\zeta^2)^{1/2}\int_0^\infty \left[H_1(s)(\tanh\alpha s - \tanh\beta s) + \frac{2}{1+\mathrm{e}^{2\beta s}}\right]\cosh s\xi J_0(s\zeta)\mathrm{d}s, \quad \mathbf{x}\in\Omega_0 \\ c &= (\xi^2+\zeta^2)^{1/2}\int_0^\infty \left[H_1(s)(\tanh s\xi - \tanh\beta s) + \frac{2}{1+\mathrm{e}^{2\beta s}}\right]\cosh s\xi J_0(s\zeta)\mathrm{d}s, \quad \mathbf{x}\in\Omega_1. \end{aligned} \tag{B.2}$$

Substituting (B.2) into boundary condition (4) results, after certain manipulations (Leshansky et al., 1997), in the following integral equation for function $H_1(s)$:

$$H_1(s) = f_1(s)\int_0^s H_1(v)\Phi_1(v)\mathrm{d}v + f_2(s)\int_s^\infty H_1(v)\Phi_2(v)\mathrm{d}v + \Phi_0(s),$$

$$f_1(s) = \frac{K_0(\beta s)}{\varphi_1(s)}, \quad f_2(s) = \frac{I_0(\beta s)}{\varphi_1(s)}, \quad \Phi_1(s) = I_0(\beta s)\varphi(s), \quad \Phi_2(s) = K_0(\beta s)\varphi(s),$$

$$\varphi_1(s) = \alpha[\tanh\alpha s + (\kappa-1)\tanh\beta s]\sinh\alpha s - \kappa\alpha\cosh\alpha s,$$

$$\varphi(s) = [\tanh\alpha s + (\kappa-1)\tanh\beta s]\cosh\alpha s - \kappa\sinh\alpha s,$$

$$\Phi_0(s) = \frac{2(1-\kappa)}{\varphi_1(s)}\left[\frac{\alpha\sinh\alpha s}{1+\mathrm{e}^{2\beta s}} + K_0(\beta s)\int_0^s \frac{\cosh\alpha v}{1+\mathrm{e}^{2\beta v}} I_0(\beta v)\mathrm{d}v + I_0(\beta s)\int_s^\infty \frac{\cosh\alpha v}{1+\mathrm{e}^{2\beta v}} K_0(\beta v)\mathrm{d}v\right],$$

where $I_0(x)$ and $K_0(x)$ are the modified Bessel function of the first kind and the McDonald function, respectively.

This integral equation is equivalent to the following linear ordinary differential equation and boundary conditions:

$$g_2(s)\frac{\mathrm{d}^2H_1}{\mathrm{d}s^2} + g_1(s)\frac{\mathrm{d}H_1}{\mathrm{d}s} + g_0(s)H_1 = g(s), \quad \frac{\mathrm{d}H_1}{\mathrm{d}s} = 0,\ s=0;\ H_1\to 0,\ s\to\infty$$

with

$$g(s) = \frac{2(1-\kappa)\mathrm{e}^{2\beta s}}{(1+\mathrm{e}^{2\beta s})^3}\left[(\mathrm{e}^{2\beta s}s - \mathrm{e}^{2\beta s} - s - 1)\sinh\alpha s - 2\alpha s(1+\mathrm{e}^{2\beta s})\cosh\alpha s\right],$$

$$g_0(s) = s\frac{d^2\varphi_1(s)}{ds^2} + \frac{d\varphi_1(s)}{ds} - s\varphi(s),\ g_1(s) = \varphi_1(s) + 2s\frac{d\varphi_1(s)}{ds},\ g_2(s) = s\varphi_1(s)$$

and $H_1(s)$ satisfying

$$H_1(0) = 2\alpha(1-\kappa)\int_0^\infty \frac{\cosh \alpha s}{1+e^{2\beta s}} K_0(\alpha s)ds - \alpha\int_0^\infty H_1(s)\varphi(s)K_0(\alpha s)ds.$$

This problem can be solved numerically as described in Leshansky et al. (1997). As soon as the concentration on the boundary is known, substituting presentation (30)–(32) into boundary conditions (15)–(17) results in a following set of linear algebraic equations on the functions $A(s), B(s), C(s), D(s), A_0(s), C_0(s), A_2(s)$ and $C_2(s)$.

$$A(s)\sinh \alpha s + B(s)\alpha \sinh \alpha s + C(s)\cosh \alpha s + D(s)\alpha \cosh \alpha s = 0,$$

$$A(s)\sinh \beta s + B(s)\beta \sinh \beta s + C(s)\cosh \beta s + D(s)\beta \cosh \beta s = 0,$$

$$A_2(s) + C_2(s)\beta = 0,\ A_0(s) + C_0(s)\beta = -\frac{1}{2}e^{-2s\beta}\left(\beta + \frac{1}{s}\right)V_1,$$

$$A(s)s + C(s)s\tanh \beta s + B(s)(\beta s + \tanh \beta s) + D(s)(1 + \beta s\tanh \beta s) = \frac{A_2(s)}{1+2e^{2\beta s}},$$

$$\mu_1(C(s)\cosh \beta c + D(s)\sinh \beta s) = -2\mu_2 e^{-\beta s}C_2(s),$$

$$A(s)s + C(s)s\tanh \alpha s + B(s)(\alpha s + \tanh \alpha s) + D(s)(1 + s\alpha\tanh \alpha s) = \frac{A_2(s)}{1+2e^{-2\alpha s}} - \frac{2\alpha s+1}{1+2e^{2\alpha s}}V_1,$$

$$\mu_1(C(s)\cosh \alpha c + D(s)\sinh \alpha s) - 2e^{\alpha s}C_0(s) = -\frac{e^{-\alpha s}}{2}V_1 + \frac{1}{\alpha}\left(\cosh \alpha s\frac{dH(s)}{ds} - \sinh \alpha s\frac{dK(s)}{ds}\right).$$

References

Basset, A.B.A., 1888. Treatise on Hydrodynamics, 2. Deighton Bell, Cambridge.

Berejnov, V., Leshansky, A.M., Lavrenteva, O.M., Nir, A., 2002. Spontaneous thermocapillary interaction of drops: effect of surface deformations at non-zero capillary number. Phys. Fluids 14, 1326–1339.

Chen, J., Stebe, K.J., 1997. Surfactant-induced retardation of the thermocapillary migration of a droplet. J. Fluid Mech. 340, 35–59.

Chervenivanova, E., Zapryanov, Z., 1989. On the deformation of compound multiphase drops at low Reynolds numbers. PhysicoChem. Hydrodyn. 11, 243–259.
Cooley, M.D.A., O'Neil, M.E., 1969. On the slow motion of two spheres in contact along their line of centers through a viscous fluid. Proc. Cambridge Philos. Soc. 66, 407–413.
Edwards, D.A., Brenner, H., Wasan, D.T., 1991. Interfacial Transport Processes and Rheology. Butterworth-Heinemann, Maddschusets.
Golovin, A.A., Nir, A., Pismen, L.P., 1995. Spontaneous motion of two droplets caused by mass transfer. Ind. Eng. Chem. Res., 3278–3288.
Happel, J., Brenner, H., 1965. Low Reynolds Number Hydrodynamics. Prentice-Hall, Englewood Cliffs, NJ.
Kan, H.C., Shyy, W., Udaykumar, H.S., Vingeron, P., Tran Son Tay, R., 1999. Effects of nucleus on leukocyte recovery. Ann. Biomed. Eng. 27, 648–655.
Kan, H.C., Udaykumar, H.S., Shyy, W., Tran Son Tay, R., 1998. Hydrodynamics of a compound drop with application to leukocyte modeling. Phys. Fluids 10, 760–774.
Landman, K., 1983. On the crenation of a compound liquid droplet. Stud. Appl. Math. 69, 51 (Math lib).
Landman, K., 1985. Stability of a viscous compound drop. AIChE 31, 373–567.
Lavrenteva, O.M., Leshansky, A.M., Nir, A., 1999. Spontaneous thermocapillary interaction of drops, bubbles and particles: unsteady convective effects at low Peclet numbers. Phys. Fluids 11, 1768–1780.
Lavrenteva, O.M., Nir, A., 2001. Spontaneous thermocapillary interaction of drops: unsteady convective effects at high Peclet numbers. Phys. Fluids 13, 368–381.
Lavrenteva, O.M., Berejnov, V., Leshansky, A.M., Nir, A., 2002. Spontaneous interaction of drops, bubbles and particles in viscous fluid driven by capillary inhomogeneities. Ind. Eng. Chem. Res. 41, 357–366.
Leshansky, A.M., Golovin, A.A., Nir, A., 1997. Thermocapillary interaction of a solid particle and a liquid-gas interface. Phys. of Fluids 9, 2818–2827.
Leshansky, A.M., Lavrenteva, O.M., Nir, A., 2001. Thermocapillary migration of bubbles: convective effect at low Peclet numbers. J. Fluid Mech. 443, 377–401.
Leshansky, A.M., Lavrenteva, O.M., Nir, A., 2003. The weakly inertial settling of particles in a viscous fluid. R. Soc. Proc. A 459, 3079–3098.
Leshansky, A.M., Lavrenteva, O.M., Nir, A., 2004. The leading effect of fluid inertia on the motion of rigid bodies at low Reynolds number. J. Fluid Mech. 505, 235–248.
Loewenberg, M., Davis, R., 1993. Near-contact thermocapillary motion of two non-conducting drops. J. Fluid Mech. 256, 107–131.
Lyell, M.J., Carpenter, M.J., 1993. The effect of residual contamination on Marangoni convection in a spherical liquid system. Appl. Sci. Res. 14, 639–662.
Morton, D.S., Subramanian, R.S., Balasubramaniam, R., 1990. The migration of a compound drop due to thermocapillarity. Phys. Fluids A 2, 2119–2133.
Nir, A., Lavrenteva, O.M., 2003. Capsule dynamics and interfacial transport. In: Modeling and Simulation of Capsules and Biological Cells. CRC Press, pp. 197–262.
Oseen, C.W., 1927. Hydrodynamik. Akademische Verlagsgesellschaft, Leipzig.
Sadhal, S.S., Oguz, H.N., 1985. Stokes flow past compound multiphase drops: the case of completely engulfed drops/bubbles. J. Fluid Mech. 160, 511–529.
Sideman, S., Moalem-Maron, D., 1982. Direct contact condensation. Adv. Heat Transfer 15, 228–281.
Stimson, M., Jeffrey, G.B., 1926. The motion of two spheres in viscous fluid. Proc. R. Soc. A 111, 110–116.
Stone, H.A., Leal, L.G., 1990. Breakup of concentric double emulsion in linear flow. J. Fluid Mech. 211, 123–156.
Subramanian, R.S., Balasubramaniam, R., 2001. The Motion of Bubbles and Drops in Reduced Gravity. Cambridge University Press.
Van Dyke, M., 1975. Perturbation methods in fluid mechanics. Parabolic Press.
Yiantsios, S.G., Davis, R.H., 1990. On the buoyancy-driven motion of a drop towards a rigid surface or a deformable interface. J. Fluid Mech. 217, 547–573.